3.2.4.1 'Masking'

For many of the procedures detailed, it is necessary to 'mask' the data. In essence, this removes unwanted data from the image. In the example below, a printed dot is shown, masked, and unmasked, Figure 3-9.

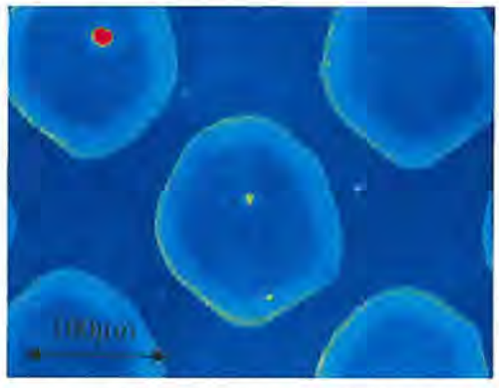

Figure 3-9 – unmasked

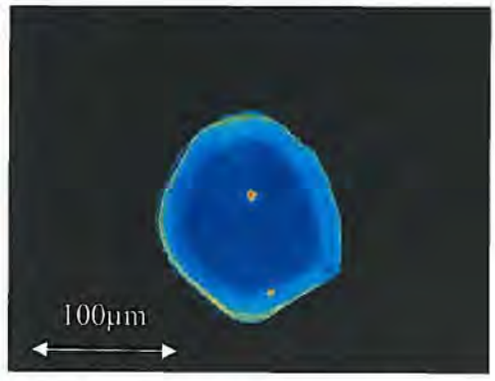

Figure 3-9 – masked

Figure 3-9 – Masked and unmasked images

Masking may be performed automatically, by height, co-ordinate, or by defining either a specified shape (rectangle, circle etc) or by defining an irregular polygon, as required. The technique is used to isolate cells (see Appendix 1), or to isolate dots (see section 4.4.2.4) as well as to remove rogue data from measurements. For the analysis of dots, polygons were created to isolate the dot. In the case of cells, either a polygon or a circle was used depending on the size of the cells, and the amount of space surrounding the detail in question.

3.2.5 Cell Volume

Three different interferometers were available for use, and were used as appropriate. The first is a large, laboratory based interferometer. The interferometer itself is based on an air-table, minimising vibration, and offers the highest flexibility. Multiple internal magnifications are available, and several lenses may be mounted on the measurement turret. This interferometer was used in the analysis of diamonds. Although it is the most flexible in terms of measurement options, it is not possible to

mount a gravure cylinder under the measurement turret. The second is a portable unit. Utilising no internal magnification, and a CCD camera of the same resolution as the laboratory based unit this device was used primarily for measurements taken on cylinders (cells or surface finish). The third device is another portable device, utilising 0.5x internal magnification. This device uses a lower resolution CCD, offering a lower horizontal resolution, and also has a lower vertical resolution. This device was used where excess vibration occurs, as it is less sensitive to vibration than the higher resolution portable device.

As previously indicated in 3.2.3, traditional volume measurements are taken by measuring the length and width of a cell using optical microscopy, and inferring a volume from these measurements and the stylus angle. Microscope images of cells are shown in Figure 3-10 – below.

Figure 3-10 – Microscope image of cell

If the stylus angle, θ, is known, the volume of the cell is calculated, using the formula;

$$volume = \left(\frac{height \times width}{2}\right) \times \left(\frac{width}{2\tan(\theta/2)}\right) \times \frac{1}{3}$$

Equation 3.1 – Traditional volume calculation

Results from this formula will be compared with results generated from the method that was developed based on actual cell geometry measurement.

As a starting point, measurement of engraved cells made with the system as supplied is shown in Figure 3-11. Due to low reflectance, optical noise and an inability of the

lens to collect light back from the sloped cell sides, approximately 99% of the data from inside the cell is missing (left image).

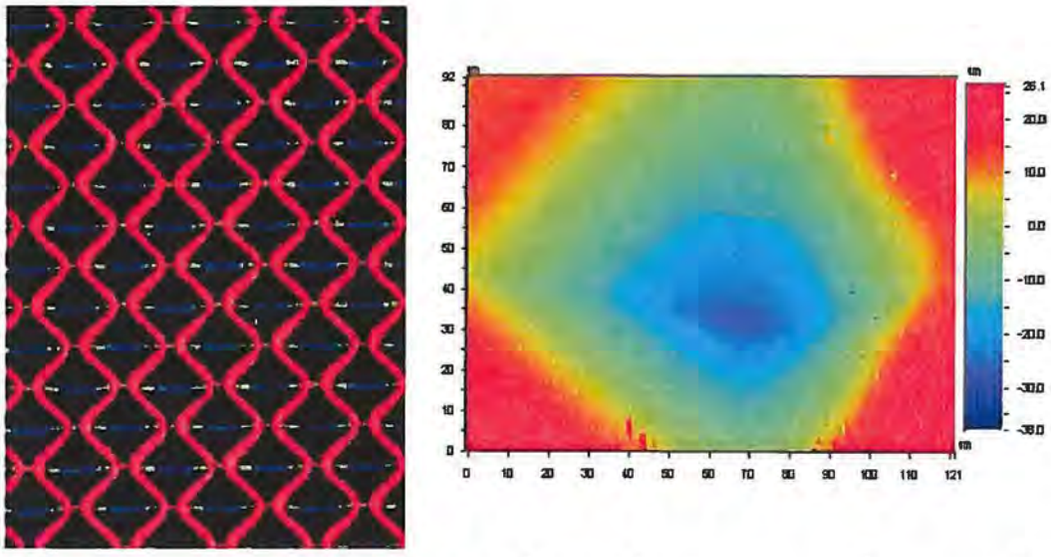

Figure 3-11 – **Interferometric measurement of gravure cells**

In the example shown above (Figure 3-11), black indicates missing data. The only information available for calculation is the apex of the cell and the base corresponding to the roll surface. There is a requirement to interpolate the remaining data to calculate the volume within the cell. Also in Figure 3-11, the right hand image shows a measurement taken with an improved optical system. Now 99% of the data from inside the cell is present, and calculation of actual volumes based on measurement can be performed, rather than inferring it. The optical configuration was improved by using a higher magnification lens. This allowed the measurement of sloped surfaces (such as the inside of a cell) and by minimising the number of cells being measured, the amount of optical noise is reduced.

Because the sides of the cells are sloped, most of the light is not reflected back up into the interferometer, but bounces off the other walls, causing optical noise. By increasing the intensity, and decreasing the number of cells, the opportunity for noise is reduced, and more light is reflected from the cell walls, allowing measurement (Figure 3-11, right hand image). With this much higher data rate, this allows accurate calculation of volume rather than the inferences, which are characteristic of previous works.

Previously several different possible techniques had been attempted, including coating the surfaces with carbon to reduce the reflectance, and minimise noise, and by removing filters from within the interferometer, to reduce the coherence length, and thus improve the sensitivity of the interferometer to measure the sloped cell walls. However, these methods had not provided data of sufficient quality to facilitate actual volume measurement.

An analysis package was supplied with the interferometer to allow calculation of the specific volume of anilox rolls. This may, according to documentation, also be used for analysis of gravure cells. However, several assumptions are embodied in the measurement and data reduction. The analysis package's volume measurement system was re-evaluated with the new optical system. A much higher data rate was achieved, covering just one cell, however as the automatic analysis needs at lest 16 cells, calculations could not be performed using the supplied analysis package. It was also discovered on analysis of the automatic function that incorrect values (for example, an unrealistic cell volume) are often calculated for reasons that could not be established. Therefore a new methodology was required.

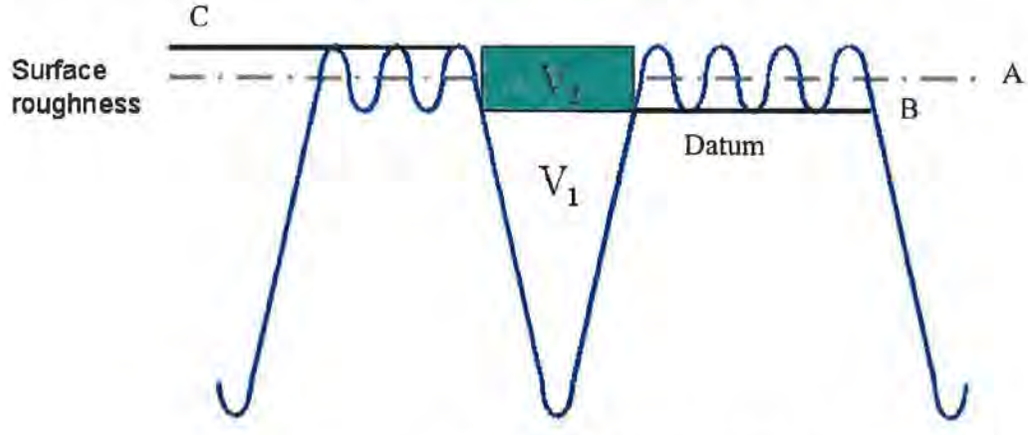

Figure 3-12 – Diagram of Surface and Cell

To facilitate accurate volume measurement, roll surface roughness needs to be taken into account, see **Figure 3-12**. If the volume was calculated below level 'c' this would include volume in the land surface of the cylinder in addition to the cell volume. Therefore before a volume measurement can be calculated, a series of surface levels

must be defined, the volume below which can be calculated. The total volume required will be the sum of volume V_1 and volume V_2 in Figure 3-12 – i.e. from the apex of the cell to level 'C'. It is necessary first however, to define the 'land level' – i.e. the modal height for the unengraved, top surface of the cylinder, level 'A' in Figure 3-12 which can be simply established from analysis of the data. However, using this datum line for volume calculation includes volume from the top surface of the cylinder in the measurement, which is not part of the cell volume. As a result of this the datum for volume measurement was redefined to level B, by stating that:

$$\text{Datum height} = \text{Average land height} - \tfrac{1}{2} R_z$$

Equation 3.2 – Datum height calculation

Part of the cell is formed below this datum (Figure 3-12 – volume V_1), and that anything above it is merely a part of the cylinders own roughness – barring the space above the actual cell (Figure 3-12 – volume V_2). Data above the datum line (indicated by line 'B' in Figure 3-12) must be removed for volume measurement. This removes the land area from the measurement, leaving only the cell. Should the measurement contain other cells or parts of cells, these must also be removed, using the masking facility.

To compute measured volume, the area of a single pixel is calculated, and multiplied by the depth from the datum height in the measurement. This result is then integrated across the entire measurement field to give a total volume (V_1) for the cell. This is an automated function, built into the analysis package supplied. The correctness of its working was confirmed via the use of a stepped surface[7], and was found to be accurate.

This volume does not yet represent the volume of the engraved cell. The top part of the cell has been removed in order to remove the land area (volume V_2), and this

[7] The stepped surface used was an extremely smooth and accurately defined step, used for calibration of the equipment, As the dimensions of the step are well specified by the manufacturers, the volume can be calculated mathematically and by the measurement technique.

needs to be added back in to calculate the final cell volume. This section is calculated using the open area of the cell (section 3.2.6). This is multiplied by the R_z to give volume V_2, Figure 3-12, which when added to the cell volume previously calculated (V_1) gives a total volume for the cell. A further section is missing around the very top section of the cell, indicated by the space between the volume V_2 and the surface roughness in Figure 3-12. This was calculated as being between 0.3% for a small cell, to 0.1% for a larger cell. This is negligible, and was excluded in the analysis.

Primary work was undertaken to calculate the number of cells that must be evaluated in order to provide an acceptable average. An example of this type of calculation is given in section 3.6 (for the number of analysed dots). It was found that the analysis of four cells was required. For each analysis of each type of cell, five were measured the additional cell being included to ensure that enough measurements were obtained in the event of a problem with one of the measurements, and results were then averaged. An example of calculation of all parameters is given at the end of this section.

3.2.6 Cell length, width depth and open area

With the measurement area masked for the volume calculation (see 3.2.5), the length and width of the cell was also calculated. Length is determined as the distance between the point at which the diamond enters the copper to engrave the cell, to the point at which it leaves. This is indicated by length 'a' in Figure 3-13. The width is defined as the maximum distance between points in the cross-cylinder direction. This is indicated by length 'b' in Figure 3-13. It was taken to be a simple linear measure, the curvature of the cylinder making little difference to the length on these scales. The dimension 'A' is however, not determined by diamond geometry , but by the speed at which the diamond is pushed into the copper, and the speed of rotation of the cylinder during the engraving process.

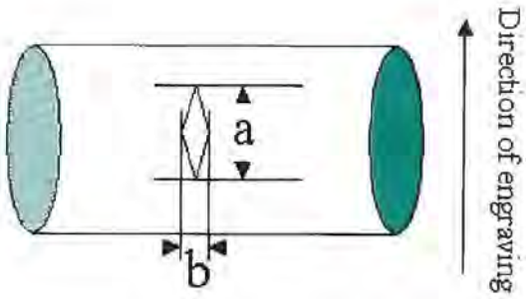

Figure 3-13 – Width and Length calculation

If all data *above* the datum line is masked, as in 3.2.5 (volume calculation) the number of measurement points making up the cell can be measured. By multiplying the number of pixels by the area of each pixel, the open area of the cell may be calculated (Equation 3.3)

$$Open\_Area = \sum N_p \times P_a$$

Equation 3.3 – Open area calculation

The measured depth of a cell is the vertical distance from line 'A' to the base of the cell in **Figure 3-12**. The actual depth of the cell must also include the 0.5 R_z that was subtracted by the manual masking. (see section 3.2.5). Adding this 0.5 R_z on to the depth ensures that the top and bottom of the cell are in the same place for both volume and depth calculations.

3.2.7 Cell offset

Due to the electromechanical engraving technique used in the production of the cylinder the lowest point in the cell is not precisely in the middle of the cell. The offset angle defines the angle between a vertical line from the bottom of the cell and the line joining the bottom of the cell to the geographical centre of the cell. The offset is directly related to the diamond and its holder used in the engraving. A typical

example of the type used is shown below (Figure 3-14). The diamond is rotated into the copper about the pivot point. As a result, the diamond tip does not execute a straight line as it enters the copper, but a curve, which shows itself as the measured offset value.

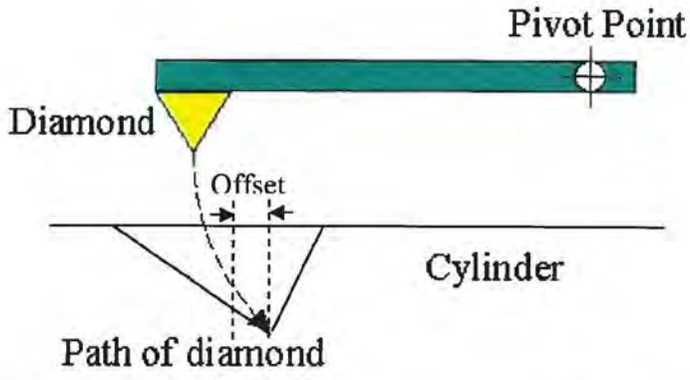

Figure 3-14 – Engraving Diamond

This can be seen most clearly if the cell data is inverted, Figure 3-15.

Figure 3-15 – Inverted cell, showing offset

The offset is indicated by the manner in which the cell 'leans' to the right.

3.2.8 Cell wall roughness

Once a cell has been measured, it is possible to select only a small portion of the cell, and flatten it in the measurement plane through the application of a mask (section 3.2.4.1). From this, it is possible to calculate the roughness of the wall inside the cell.

An example is shown in Figure 3-16. A preliminary investigation was performed. Although it highlighted internal cell features, it did not affect cell volume significantly and so was not considered to be important in the context of this study.

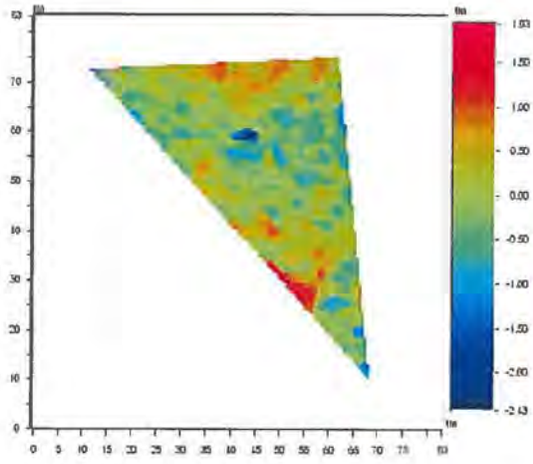

Figure 3-16 – Cell wall quadrant, showing roughness

3.2.9 Example calculation

A typical measurement is shown below, Figure 3-17. Several cells are included in the measurement, and the measurement must be masked to remove the additional cells.

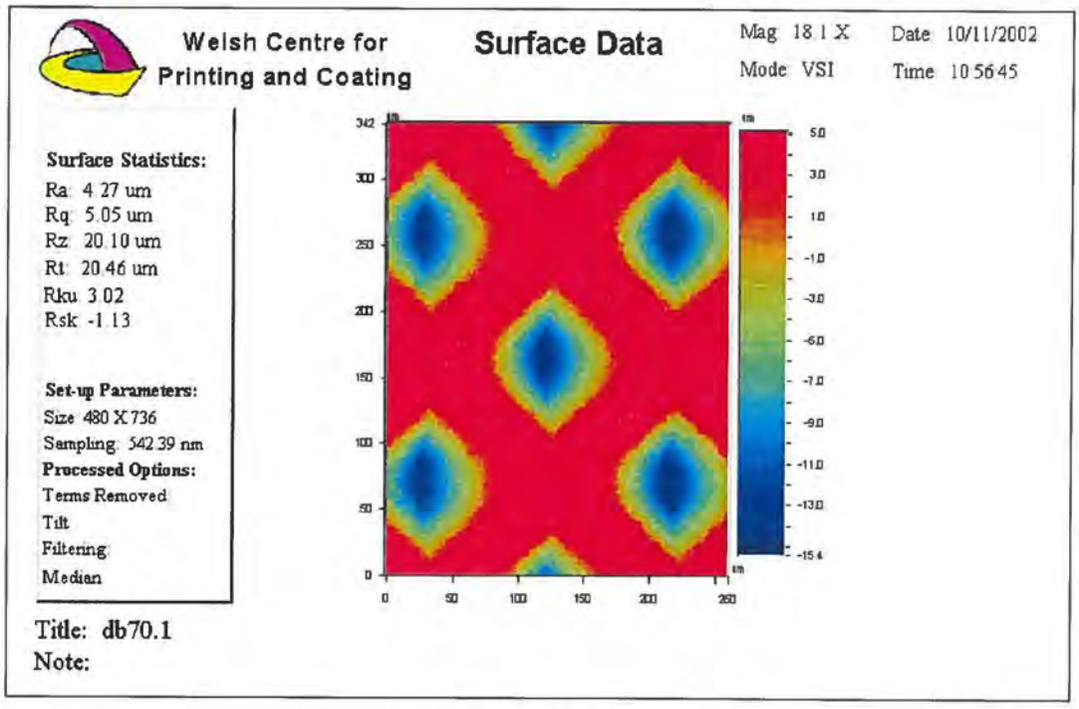

Figure 3-17 – Raw measurement of engraved surface

Figure 3-18 shows the individual cell to be analysed. This has been masked, removing the extra cells,. The shape of the mask is not critical, and here a simple circle has been used to isolate the cell.

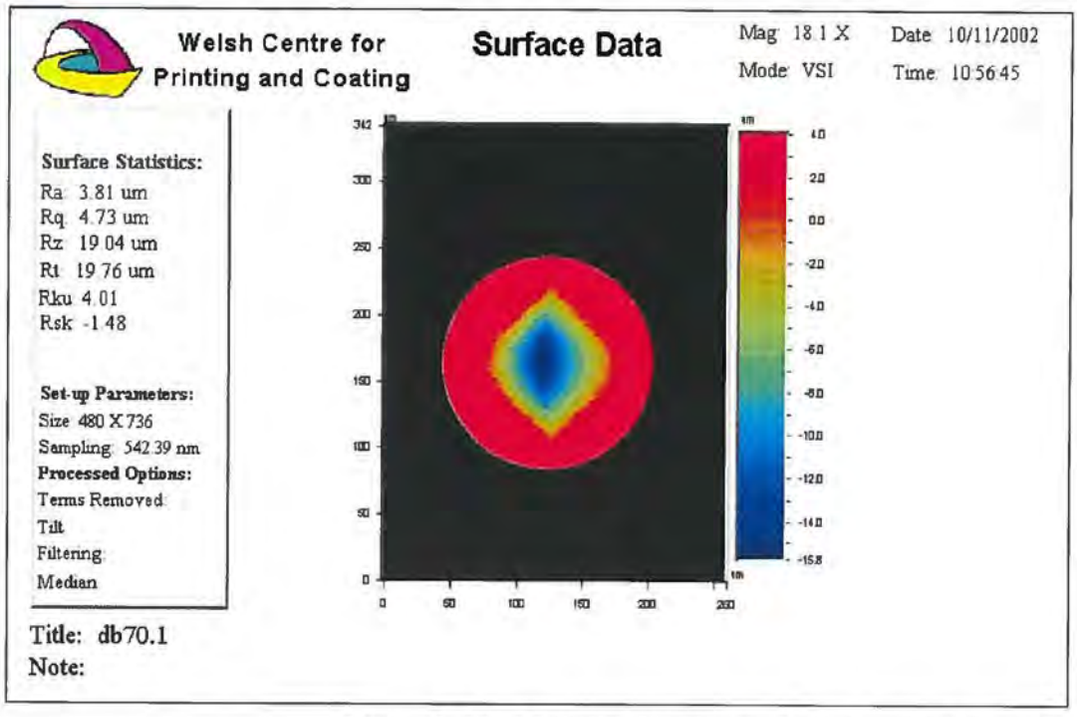

Figure 3-18 - Masked measurement of engraved surface

A measurement screen was set up to allow calculation of depth and volume, Figure 3-19. This incorporates both a 2D image of the cell, (top left), a volume chart (top middle – unused), the volume information (top right) and a histogram, (bottom).

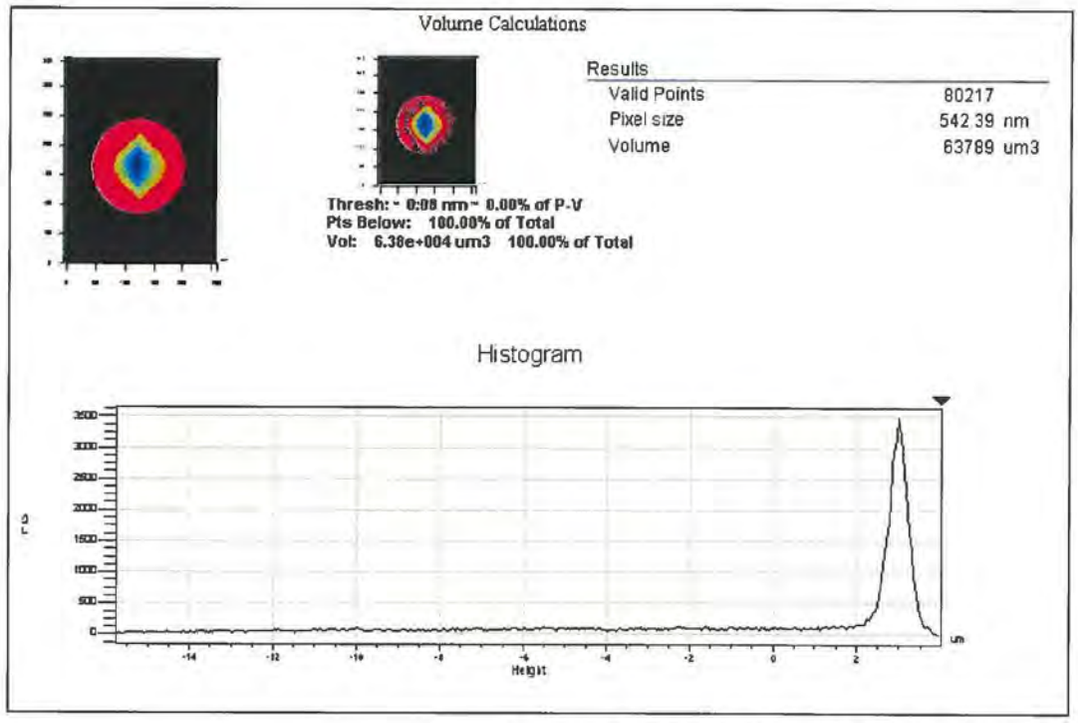

Figure 3-19 – Developed calculation screen

The histogram (at the bottom of the screen) shows the number of points at any given height. The 'Volume' number is the number of cubic microns of fluid which would be required to submerge the sample to the highest point on it. This is equivalent to the volume described in section 3.2.5 as the volume below line 'C' (**Figure 3-12**) The 'Valid Points' variable, gives the number of pixels in the measurement.

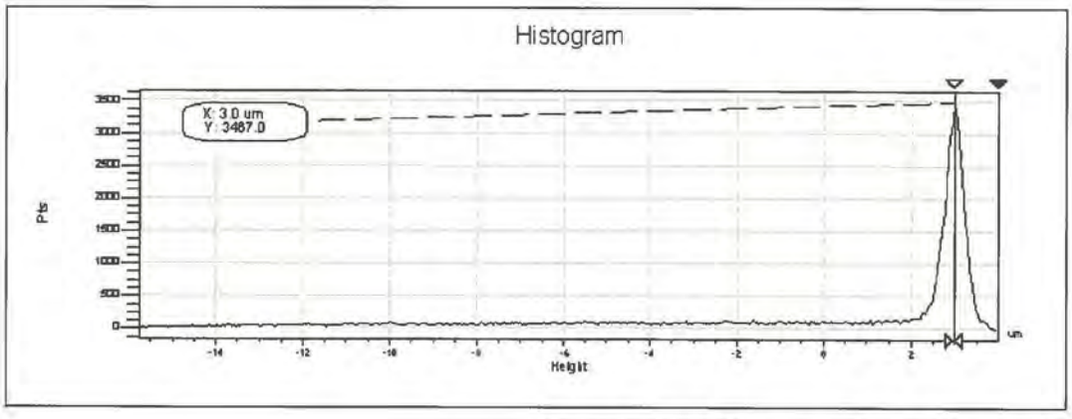

Figure 3-20 – Histogram indicating peak

In Figure 3-20 the highest point indicates the most common height for pixels – in this case, relating to the height of the land area.

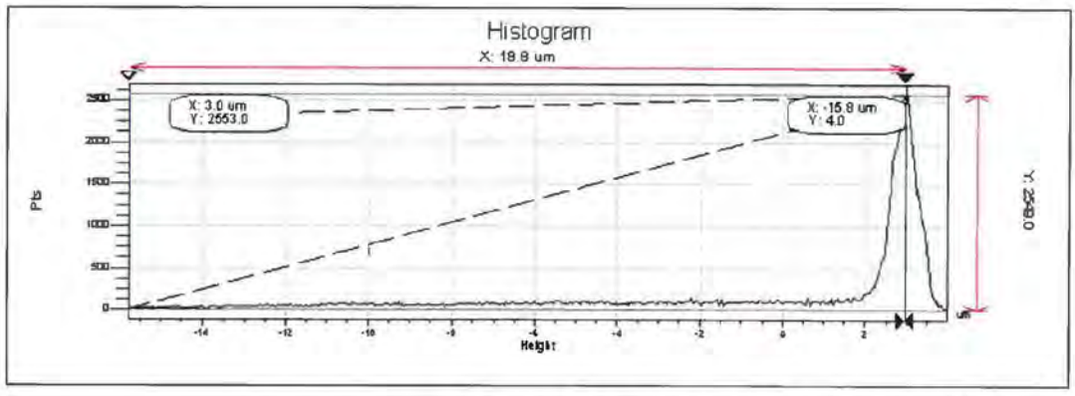

Figure 3-21 – Histogram, indicating cell depth

The height from the land area to the lowest data point gives the depth of the cell, minus the ½ Rz, which for this cylinder = 0.8µm above the mean land level, thus the total depth of the cell is 19.6µm, Figure 3-21 (18.8µm as indicated, + 0.8µm = 19.6µm)

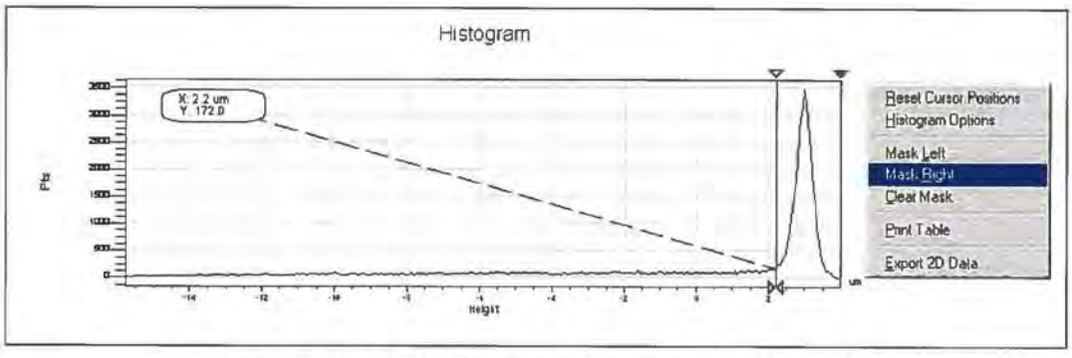

Figure 3-22 – Histogram indicating masking point and direction

The cursor has now been moved 0.8µm to the left (down), and a 'Mask Right' is about to be performed. This removes all data to the right (above) of the cursor, Figure 3-22. This leaves the part of the cell below line 'B' in **Figure 3-12**. As stated above, 0.8µm is equivalent to ½ Rz for this cylinder.

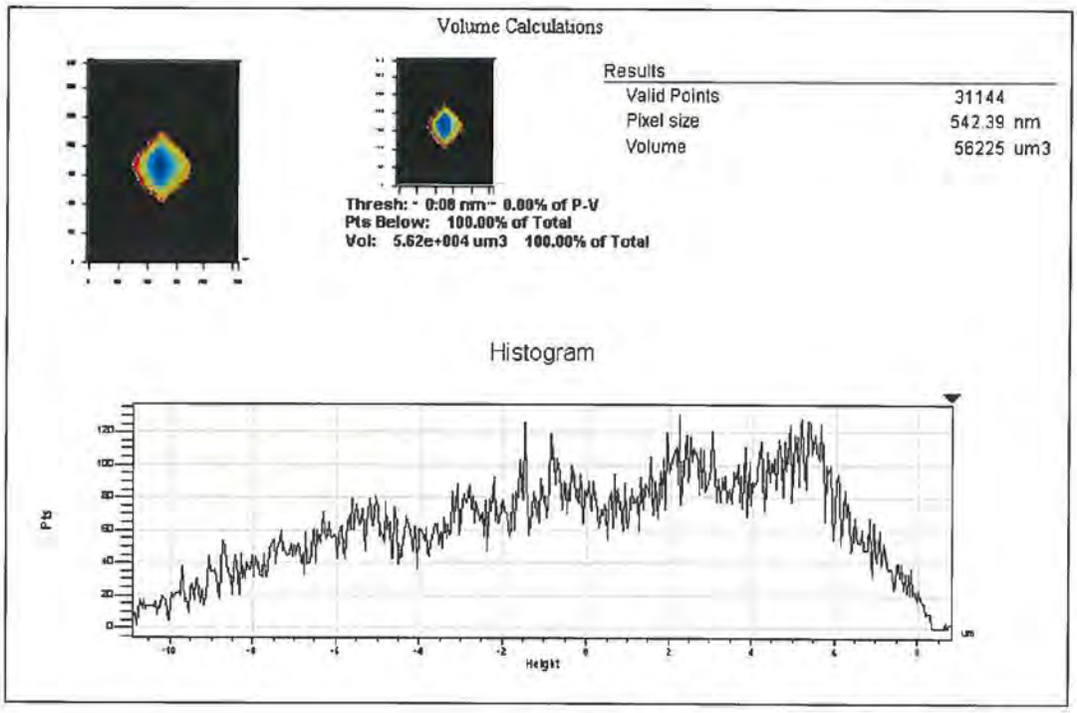

Figure 3-23 – Entire data for masked cell

The volume (V_1) for the cell may now be calculated using data taken from the analysis package, Figure 3-23. In this case;

- Volume = 56225um^3
- Valid Points = 31144 points

The area of this open area must now be calculated. The total measurement area is equal to

$$342 \text{ um} \times 260\text{um} = 88920\text{um}^2$$

using a camera of resolution 736x480 pixels. Thus 1 pixel equals;

$$\frac{342 \times 260}{736 \times 480} = 0.252 \text{ um}^2/\text{pixel}$$

Thus

Total Volume = Volume of cell + Volume of top section

Total Volume = Volume of cell + (Open area x R_z)

Total Volume = Volume of cell + (Valid Points x Area/pixel x 1.6)

Total Volume = 56225 + (31144 x 0.252 x 1.6)

Total Volume = 68,782um^3 for this cell

The cell dimensions may be established using a similar strategy, Figure 3-24.

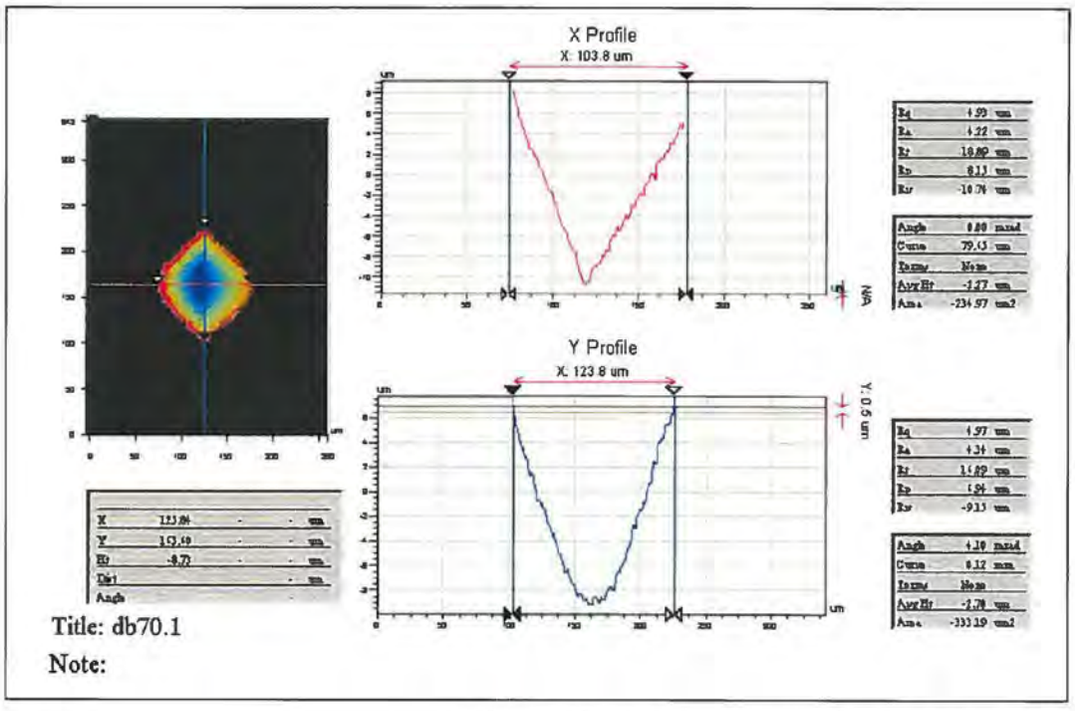

Figure 3-24 – Measurement of depth and width

Here the length and width of the cell may be calculated, by finding the north, south, east and west extremes of the cell (indicated by the triangles in the cell picture, top left). The width is defined as the measured distance in the 'X Profile' (103.8um) and the length as the measured distance in the 'Y Profile' (123.8um).

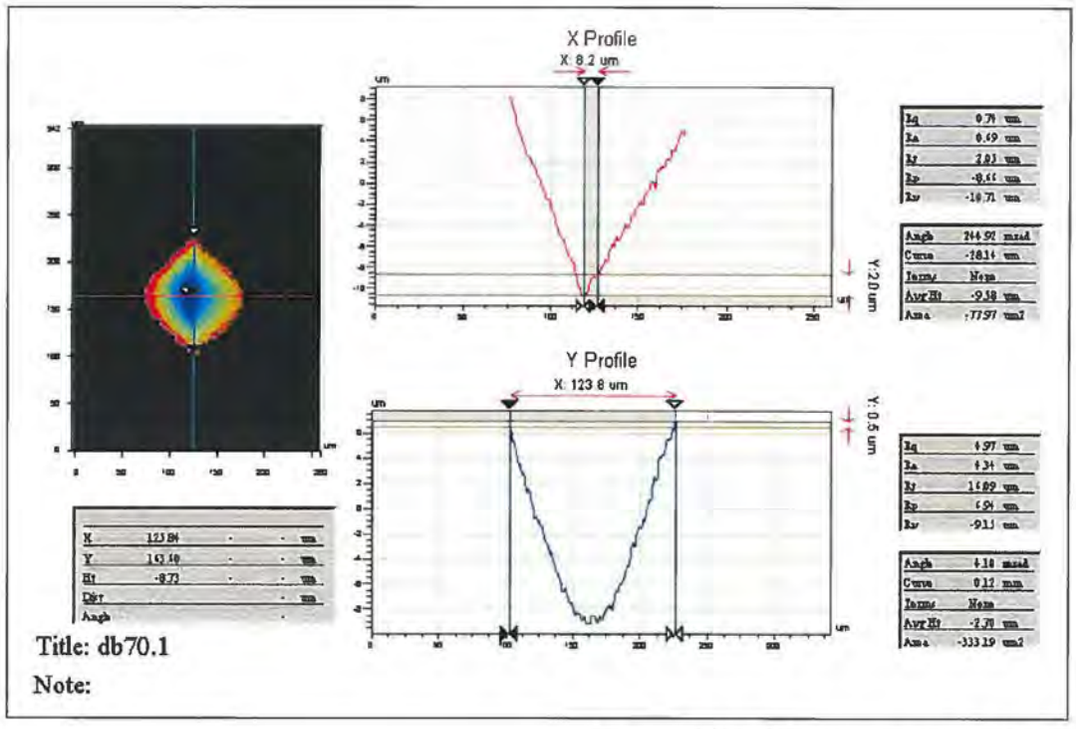

Figure 3-25 – Measurement of offset

The offset is calculated in Figure 3-25. The top of the cell is the point at which the diamond enters the copper (engraving from top to bottom) in this example, so the blue line (Y Profile) is lined up on the northmost point of the cell. The lowest point in the cell is found, and the distance in the X direction (east-west) is calculated from this point to the line coming down from the diamond entry point, in this case 8.2um.

It is also possible to measure the roughness of the internal cell walls. First, the first quadrant to be examined must be isolated, Figure 3-26. Once the quadrant is isolated, selecting the 'terms mask' allows the section isolated to be used as the measurement plane.

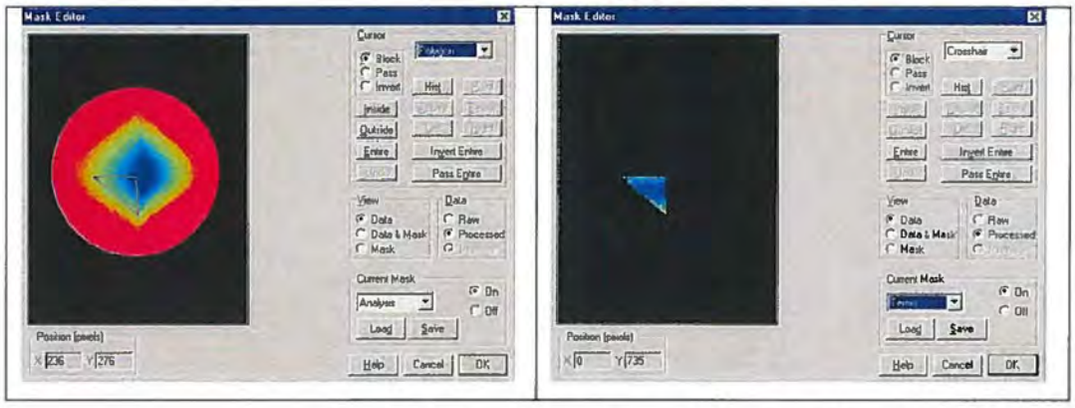

Figure 3-26 – Cell wall roughness, isolating the quadrant

Once the measurement area has been isolated, curvature must be removed, effectively rendering a level plane.

Once this has been selected, the quadrant is levelled, and the roughness, in terms of Ra, Rq etc, may be read from the analysis screen, Figure 3-27.

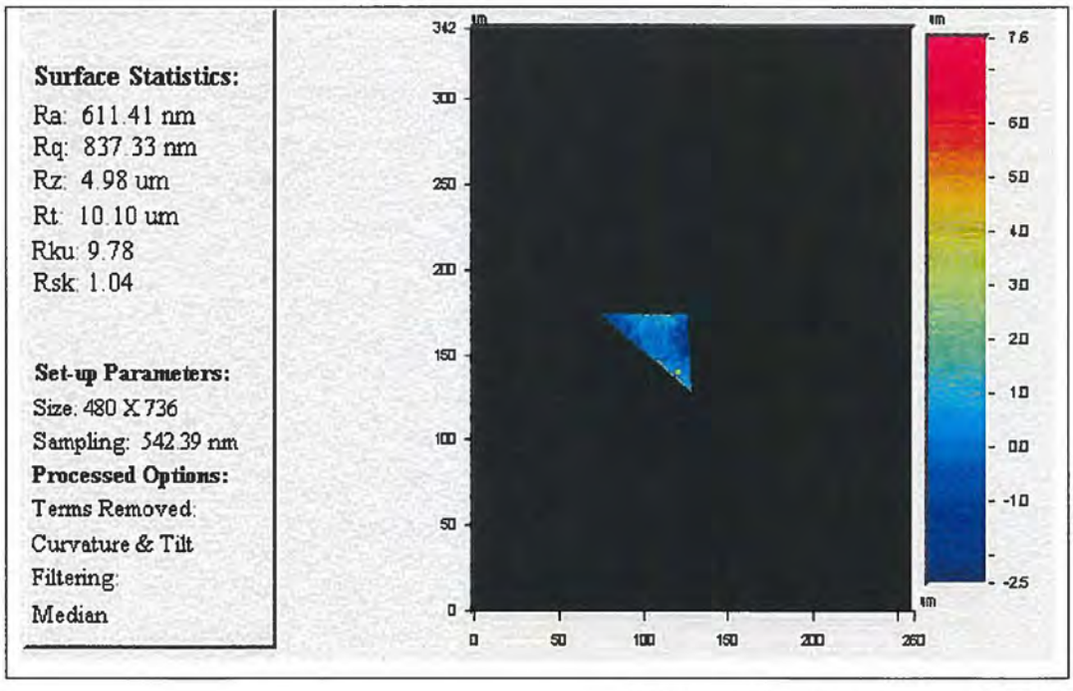

Figure 3-27 – Flattened quadrant

3.2.10 Comparison with traditional methods

A series of comparisons between different cell models was performed, to see if it was possible to use the microscopy measurements to establish the cell volume.

Calculations were performed on an 80% cell (the largest cell with no channel present), engraved with a 130° stylus. Average cell dimensions were used (137.9um wide, 153.3um long). The measured volume was compared with both the traditional, pyramid shape approximation, and a new, average circumscribing conical model where;

$$volume = \frac{\pi}{3} \times \left(\frac{width + length}{4} \right)^2 \times \frac{width}{2\tan(\theta/2)}$$

Equation 3.4 – Conical model

The possibilities of user error are much larger when using the image analysis techniques than in the measurement technique, described previously due to the necessity for user intervention when defining the width and length of cells. This may lead to inaccuracies of up to approximately 3μm in each dimension, which will have a significant effect on the results obtained.

In addition, the stylus angle must be assumed to be perfect for this calculation. Since it is shown in Appendix 1 that the diamond angle changes with wear, this adds a further inaccuracy to the calculation. Clearly this error in stylus angle is not relevant to the interferometric technique described as this measures the volume of the cell itself, without inferring the internal shape.

3.2.11 Blade load measurement

The effect of blade load on ink release was explored with the project (see figure 3.1) and a means of quantifying this is required. Practically the doctor blade is loaded on the cylinder pneumatically. The load is controlled using a gauge on the press, which

monitors the pneumatic pressure supplied to the pistons. Thus strain gauges were glued to the doctor blade, and the bending of the blade monitored. However this does not allow a direct measure of load due to the friction that is present between the blade holder and the press. This friction may be variable and therefore blade load may not be indicated consistently via the pneumatic supply pressure. The strain induced in the blade by the application of the blade to the cylinder was monitored with a PC based datalogger. This was used to ensure that the same load was applied for each trial, rather than establishing actual load levels. The latter is particularly difficult to achieve and requires the application of a calibration procedure coupled with some analysis of blade stressing [61] [62].

In the case of the scumming press trials, gauges were mounted in the centre of each surface finish band on the cylinder. This gave confirmation that the same load was being applied to each surface, with no significant variation caused by either the blade, cylinder or mounting system.

3.3 Running the Press Trials

3.3.1 Ink Release From Image Areas

Several inks are available to gravure printers, but in the UK at least, almost all gravure inks are of one of two standards, either NC (Nitrocellulose) based or PVB (Polyvinyl Butyral) based. NC inks are the most common, largely because of their lower costs, and (in the opinion of most printers) lower scumming attributes. As a result, NC inks were used for this trial.

Several different substrates were considered for the trial, from newsprint to cartonboard. The gravure industry is approximately evenly split between the use of paper and film substrates, but the packaging industry primarily uses film substrates. Due to the need to measure ink transfer, it was decided to use a plastic film. This would not absorb the ink (as most papers would) but would leave the ink on the surface of the substrate, where the volume transferred could be measured, and thus

quantified. It was decided to use a film commonly used in the industry, and as such it was agreed to use Mobil 247, white OPP (oriented poly-propylene) substrate due to its widespread usage, and thus direct commercial and practical implications for this research.

3.3.1.1 Trial Methodology

Prints were made on a standard OPP substrate using a small commercial press. The appropriate ink was loaded into the ink tray, and the press was run up to speed (100m/min). Prints were made for 60s, producing approximately 100m of print / 160 repeats of the image. Prints were collected at the end of the press on the take-up spool, and all prints were retained for analysis. Unprinted samples of substrate were also collected to allow analysis of the substrate. The speed of the press was confirmed using a handheld optical tachometer.

A series of thermocouples was used to monitor operating temperatures. They were placed on either side of the ink tray, two were attached to the frame of the press, and a further thermocouple was used to monitor ambient temperatures.

Strain gauges were attached to the doctor blade to accurately measure the applied load in three places along the length of the doctor blade, or over the width of the cylinder. Blade load measurements and thermocouple measurements were logged at a rate of 0.5Hz over the entire period of the measurements. These were used to ensure that the blade load was maintained, constant over the duration of the trial, it having been shown previously that doctor blade load / angle can make a significant difference to the printed colour / density [39] [40].

3.3.2 Ink Release From Non-Image Areas

3.3.2.1 Ink Selection

A variety of inks were selected for use. For the surface finish trial, both NC and PVB inks were used, whilst at the ink trial, three NC inks were used. NC inks were used because these are the most commonly used in the packaging industry [10] [63] [64] [65] [66]. It was decided to use standard commercial inks to ensure correlation between experimental results and practical experience. Inks were standard, commercial inks, supplied as they would be supplied to any printer, and thinned with a standard solvent. In the case of the second trial, a special 'low scum' ink was tested, but again, this was a standard ink available from the manufacturer.

The surface finish trial used black inks, while the ink trial used red inks. In each case, the inks used were produced to the same initial colour strength. They were then thinned with solvent, thus lowering the viscosity, and also lowering the colour strength. By reducing each ink to the same viscosities, colour strength was maintained at approximately similar levels.

3.3.2.2 Substrate selection

A variety of substrates were selected for use. For the first trial, three distinct substrates were chosen. A white OPP (Mobil 247 – as with the ink release from image areas trial), a clear OPP and a metallised foil. These were selected as they make up approximately 90% of the output of the printers. It was suggested that almost all scumming problems occur on plastic substrates [9] [10] [63] [64] [65] [66], so it was decided not to examine the effects on papers in this experiment.

For the second trial only two substrates were examined, the same white OPP and the same clear OPP. These were selected for the same reasons, as well as to allow direct comparison between the two trials.

3.3.2.3 Trial Methodology

Prints were made on commercial presses[8], under conditions as close to standard production conditions as possible, and conditions were replicated over the two trials. Print speed was 250m/min, and impression pressure was set at 2 bar, gauge. Blade load was set at a maximum and reduced (trial one) or at a minimum and increased (trial 2). In each case, the load was incremented by 0.25 Bar (gauge). Thus load was indicated by pressure setting on the press, and was monitored using strain gauges.

Once the press was up to speed, it was run for 45s, the blade load was incremented, the press was run for a further 45s, and the process was repeated until either scumming appeared to be eliminated, or until 0 Bar gauge pressure was being applied. The press was only stopped when necessary for ink or cylinder changes

3.4 Print Measurement Techniques

As detailed, interferometric analysis was used to quantify the features of the cylinder. Further application of this technique was used for the analysis of prints, allowing the calculation of precise dot volumes. Spectrophotometric techniques were also used, allowing the calculation of traditional values of tone gain / CIEL*a*b* colour. Measurement methodologies for colour and density measurement have been standardised, and these standard methods are described in [15]. The following sections describe the key elements.

3.4.1 Printed Density and colour

Measurements were taken with both handheld Gretag SPM-50 spectodensitometers and automated Gretag Spectrolino/Spectroscans. All results were taken using a D50 illuminant, D65 filter, and using the ANSI T standard. Transmission measurements on

[8] In each case, 10 units were available, with a printing width of approximately 1.2m. Press footprint was approximately 4m x 30m, with a height of 5m

clear substrates were taken using a Gretag Spetroscan-T transmission spectrophotometer.

3.4.1.1 Density calculation

To produce prints of differing colour, it is necessary to vary the thickness of the printed ink film. Since the rotogravure process is not a contone process, it is necessary to use an alternate method. By varying the size of the cells, and thus of the printed dots, it is possible to vary the amount of ink transferred over a given area. These different sizes of dots are referred to as halftones [19]. The density of this area measures the intensity of the printed colour. It is defined as:

$$density = \log_{10} \frac{1}{reflec\tan ce}$$

Equation 3.5 – Density calculation

3.4.1.2 Optical Tone gain calculations

When ink is transferred from the printing cylinder to the substrate, the printed dot will not in most cases be the same size as the cell from which it is printed. This change in size is referred to as the tone gain (or dot gain). Tone gain is the effect caused by the ink spreading out on the substrate, and thus giving a higher optical density than would otherwise be expected. Tone gains were calculated using the Murray-Davies equation (see Equation 3.6, below)

$$a = \frac{1 - 10^{Dt}}{1 - 10^{Ds}}$$

Equation 3.6 – Tone gain calculation

Where:

a = printed area, D_t = tonal density, D_s = solid density

In certain circumstances, the printed dot may be smaller than the cell opening. In this case, this is still referred to as tone gain, (with a negative value) and generally only occurs in the highlight regions of the image, where a very small cell is unable to transfer the ink to the substrate.

3.4.1.3 Colour difference calculations

Many different colour different calculations are available [15] [16]. For the purposes of this investigation, conventional CIELab ΔE colour difference calculations were used.

3.4.2 Scumming level measurement

In the trials it was found to be necessary to measure colour relative to that of a clean, unprinted substrate as an indicator of scumming. Initial measurements were performed using the optical density of the substrate and examining the difference between the unprinted substrate, and the printed substrate in the non-image areas. However visual examination of the scumming on some of the early samples indicated a clear green tint, despite printing being only performed with black ink. As a result of this colour measurements were used, the scumming level being indicated by the ΔE colour difference between the printed and unprinted substrate. As well as taking into effect the colour shift observed, ΔE colour differences are significantly more precise than measured densities.

3.4.3 Printed dot volume

White light interferometry was used to evaluate the volume of solid ink transferred to the substrate.

3.4.3.1 Dot volume measurement

Several different techniques for the calculation of printed dot volumes were examined. In the first instance, it was reasoned that since a cell is merely an indentation on a surface, inversion of the printed surface, Figure 3-28, should allow calculation of the dot volume, using the same method as used for calculation of an engraved cell volume. Unfortunately, although the peaks at the outside of the dot are clearly defined from the substrate (with a height, in this case of 0.7um (left) or 0.4um (right), Figure 3-29) the centre of the dot is indistinguishable from the substrate. Eventually, a technique was developed by which a measurement of a dot would be masked, removing all data but the dot itself. The data for this dot was then inverted, and the volume was calculated by the software package. In addition, this method still allows calculation of the 'open area' as the cell measurement was termed. In this case, the calculation of the printed area of a single dot is calculated.[9]

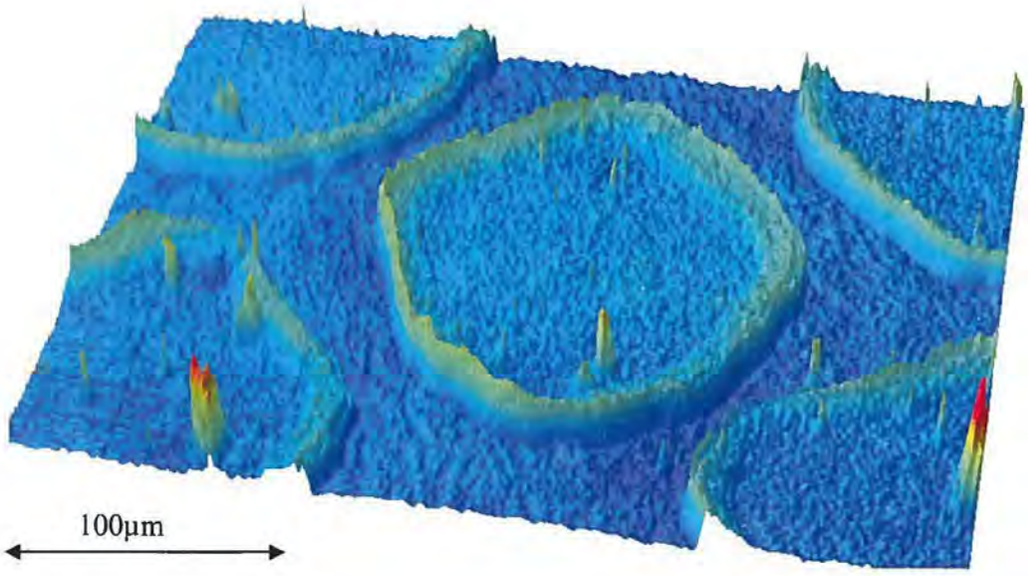

Figure 3-28 – 3D picture of gravure dot

[9] As a result of this technique it was only possible to analyse discrete dots, (such as those that appear at lower coverages). In addition, the repeatability of dots at 20% coverage and below was too poor for analysis, thus only dots at 30%, 40% and 50% coverage were analysed – 20% dots being too variable, and 60% dots joining up at the edges.

A 2D image of the dot is shown in Figure 3-29.

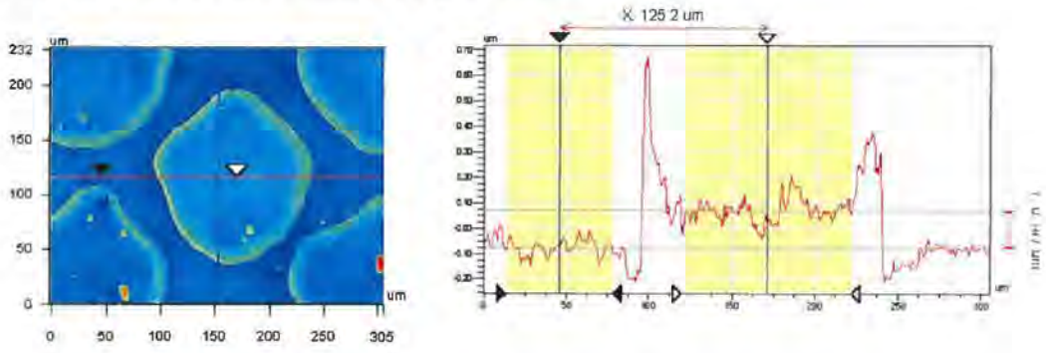

Figure 3-29 – 2D image and trace

Several problems had to be overcome when undertaking these measurements. One of the primary problems was in terms of trying to ensure the flatness of the samples. The height of the dots is so low above the surface of the substrate, that initial measurements did not allow identification of printed and unprinted areas. As a result, it became necessary to flatten the substrate. This was achieved by polishing a mirror, applying water and using surface tension to 'stick' the substrate to the surface of the mirror. It was necessary to apply this smoothly, and to ensure that no air bubbles were entrapped under the substrate, as removal of the bubbles damaged the printed surface. In addition, it was necessary to ensure the levelness of the sample. A height difference of less than 1um across the extremes of the measurement area (305 x 232um) was required for maximum precision.

The final problem relates to the optical properties of the substrate. The substrate is made up of several layers. As the interferometer scans down, light is reflected from the interface between these layers, and creates noise in the measurements. This further necessitated the sample to be maintained extremely flat on the interferometers measurement table, and required the scan to be stopped at a precise point.

3.5 Thermal Desorption – Gas Chromatography – Mass Spectrometry

Thermal Desorption - Gas Chromatography –Mass Spectrometry (TDGCMS) was used in order to ascertain the quantity of solvent in the raw substrate and the printed

substrate. When combined with the measurements of cells and printed dots, this allows calculation of the total amount of ink released from the cells. TDGCMS is a three-stage process. Thermal desorption strips the volatile component of a sample by heating. Gas chromatography separates the volatile components from the mix supplied from the thermal desorber, and mass spectrometry identifies the components from their molecular weight and measures their abundance in the measurement sample. Although there is no literature suggesting that this technique has been used previously to establish the solvent retained in a 'dry' printed ink, the manufacturers of the equipment specify that it is suitable for this sort of testing [34] [35] [36]. As discussed earlier similar experiments have been performed, using (for example) *Origanum Vulgare* leaves as a solid matrix containing volatile solvents (Garcia and Sanz [37]).

The samples used in this experiment include solid polymer substrates, both printed and unprinted and inks. Neither of these can be directly injected into the gas chromatograph. As a result it is necessary to extract the volatile solvents from the samples. This is done by heating the sample in a desorption tube while passing a stream of helium over the sample. This helium, now contaminated with the volatiles from the samples under test is passed to the gas chromatograph. This is a relatively recent technique, only used in conjunction with a gas chromatograph since approximately 1980 [67]

3.6 Statistical Confidence Confirmation

In order to ensure that the necessary number of samples were being measured in each experimental case, it was necessary to conduct a brief statistical analysis to examine the minimum sample size needed. This was performed by analysing a large number of samples (in most cases, 20) to get an accurate average. Moving average analysis was then performed on the 20 samples, to see how close the average of this reduced set was to the full set average value. A worked example of the analysis is given below, for the calculation of the number of dots required for volume analysis of printed dots.

The volume of 20 dots was measured. Indicated below.

3245	3149	2542	2356	2589
3903	3027	2732	2502	3072
2648	2597	2639	2439	2943
2714	2783	2657	2250	2496

Table 3.2 – Dot volumes (μm^3)

The average and standard deviation of this data was calculated. (Av = 2764μm^3, Standard Deviation = 377μm^3 (13.6%)). Significant variation was observed between dot volumes, and this data is representative.

Moving average analysis indicated that with 12 samples measured, a maximum error of approximately one quarter of the standard deviation was observed. Further increasing the number of samples analysed significantly increased the measurement time, without improving the accuracy. Conversely reducing the number of measurements, whilst reducing the measurement time, significantly increased the probability of introducing large errors. The numbers of measurements used are commented on in a case by case basis, in chapter 4.

Generally, the number of repeats required for confidence is high because the variability of individual dot sizes is extremely high, due to micro-variations in substrate surface energy and ink homogeneity and the number of entrained particles causing large fluctuations in dot volumes (see Figure 3-30).

Further discussion of the confidence in these measurements is given in Appendix 6, where it is shown that the size differences observed are 99.99% likely to be caused by process changes rather than measurement errors.

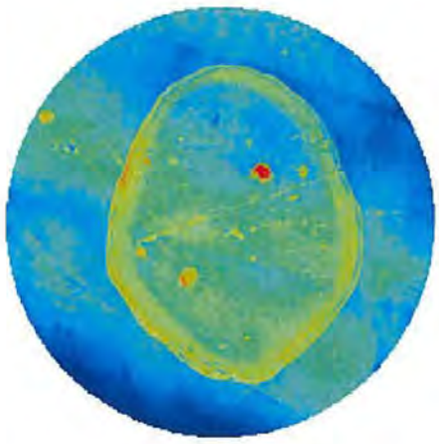

Figure 3-30a Dot – 2000um^3

Figure 3-30b Dot – 6000um^3

Figure 3-30 – Printed dots (40%, 70lpcm, 57° compression ratio, 130° stylus)

When measuring cells, it was identified that four cells were required for analysis. However, due to the nature of the measurements, although only four measurements were actually required in each case, measurement of five allowed for one measurement to be discarded as in a few cases (approximately one in twenty) a cell was found to contain a contaminant or for too much data to be missing from the image for reliable analysis to be performed. Examples are shown in Figure 3-31. The nature of the measurements necessitated this technique, each measurement taking approximately 30s, but upwards of an hour being required for overall set-up. It was thus significantly more efficient to measure an excess of data in order to be able to abandon a small fraction of the data than to measure the minimum number, and then re-measure contaminated samples.

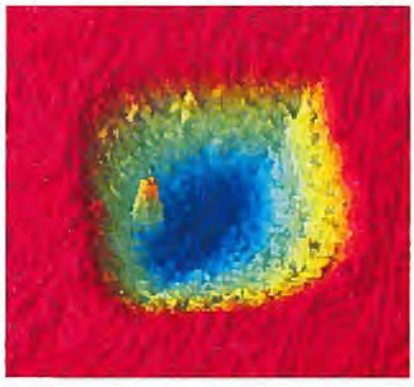

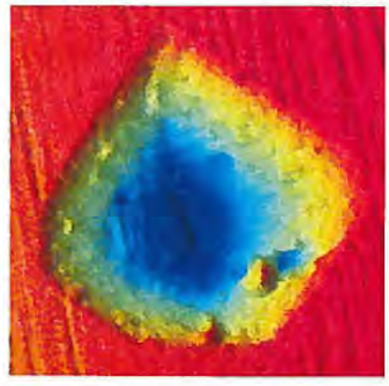

Figure 3-31 – Poor cell measurements

Contaminants, although clearly visible on results are not visible when taking the measurement, and are only discovered in post processing. The example on the left shows an otherwise good measurement, with a piece of contaminant, either dust or a little dried ink. The example on the right shows not only contaminant, but the result of poor data capture. This is clearest on the right hand side of the cell, where little definition is visible in the cell walls compared with the roughness visible in the left hand example.

3.7 Closure

This chapter has discussed, in detail the various techniques and methodologies developed in order to investigate the ink transfer from the gravure cylinder. Techniques have been demonstrated in order to accurately quantify the cells on the gravure cylinder in terms of the cell volume, depth, width, length, open area, offset and even cell wall roughness. This technique was developed and checked over a long period, and was examined by employees of the equipment manufacturer. Selected extracts of the method were also presented at users groups[10] with an interest in interferometry, demonstrating that it was possible to use an interferometer to measure inside the cells. A technique for the measurement of printed dot volume was also discussed. The application of thermal desorption – gas chromatography – mass spectrometry that was used to quantify volatile content in 'dry' printed ink was discussed.

The planning behind the selection of engraving conditions, surface finishes, ink and substrate types has been explained, along with details of the conditions, finishes, inks etc used in the course of the investigation. Novel techniques have also been developed

[10] See Appendix 4 for a list of publications and presentations generated by this work

for the analysis of engraving diamonds, allowing analysis of the cutting face and tip, as well as the stylus angle itself, and these are discussed in appendix 1.

The next chapter presents the results and discusses the findings from these tests and trials.

Chapter 4

Results and Discussion

Ink Release from Image Areas

4.1 Introduction

This chapter describes in detail, the measurement and analysis of the cylinders, engraving diamonds and prints. The purpose was to quantify the ink release from gravure cells, and to understand the fundamental mechanisms driving this transfer.

The chapter is divided into two primary sections. The first examines the details of the cylinder, and looks at the effects of changing screen ruling, stylus angle and compression ratio on the cells themselves. The second examines the prints, to investigate the quantity of ink deposited on the substrate. This part of the work uses both white light interferometry and thermal-desorption-gas-chromatography-mass-spectrometry (TDGCMS). This allows an accurate measure of ink release since retained solvents are now taken into account.

As a part of investigating how ink release is affecting the process, it is necessary to identify how several variables affect the printed density. This investigation examines the effects of stylus angle, screen ruling and compression ratio, using production inks, on a production press, using a production substrate. These results are directly comparable with those seen by gravure professionals and take the understanding of the effects of these variables into the production environment and out of the laboratory.

In addition, it should be noted that no investigations of stylus angle and compression ratio have previously been published. This is largely related to the cost of production of cylinders to investigate these variables. In addition, although the effects of screen ruling have previously been quantified, this has only been done in terms of traditional

measurements, requiring a lot of user intervention, whilst the technique used here identifies the geometric parameters of the cells independent of the user. As a result, this motivates the detailed exploration of principally geometric issues.

Finally it should be noted that the experimental program was completed using a Taguchi approach and the results were processed according to the text matrix design as explained in section 3.2.2.1. For example, analysis of screen ruling includes average values containing a balanced set of compression ratios and stylus angles.

4.2 Comparison – Traditional volume analysis with interferometric volume analysis

Traditional volume measurements, as detailed in 3.2.10 are cheap, quick and easy to perform. The technique for volume measurement, as detailed in 3.2.5 is expensive, slow and complex to perform. The new technique is however, significantly more accurate than that previously used and is a vital requirement for accurate release measurement, since all previous work on release has used an ideal (calculated) cell volume. As an illustration of its importance, a comparison between the traditional technique for volume calculation and the interferometric technique is given in Graph 4.1, and this includes the effect of line ruling, compression ratio and stylus angle.

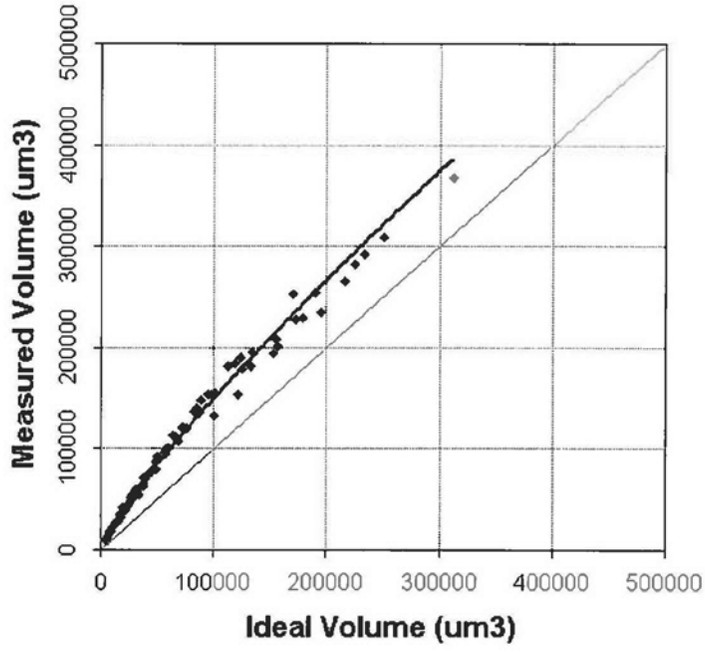

Graph 4.1 – Comparison of ideal volume and measured volume using traditional pyramidal calculation (Results for 60, 70, 80lpcm, 37, 45, 57° compression ratio, 120, 130, 140° stylus angle – all combinations)

The ideal (or calculated) volume is significantly lower than the measured volume across the entire coverage range. This is particularly the case at lower coverages, as shown in Graph 4.2 that displays the ideal volume as a percentage of the measured volume.

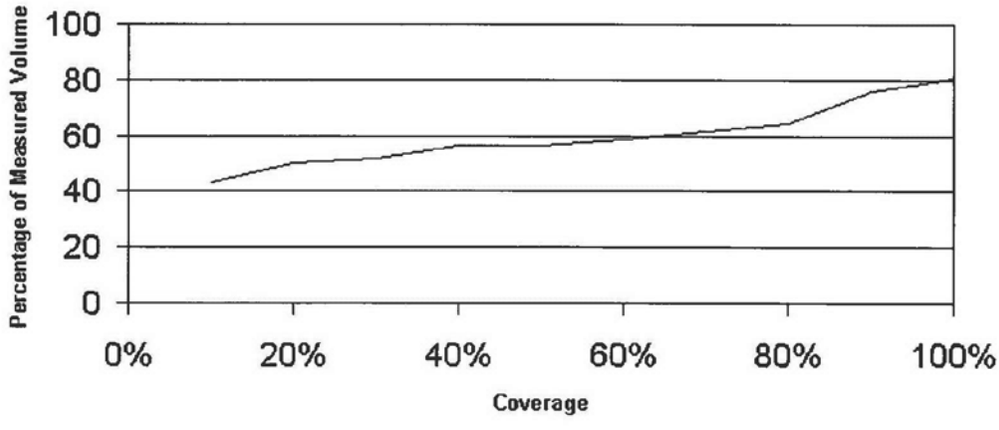

Graph 4.2 – Average deviation between measured and ideal volumes

As the coverage approaches 100%, the traditional methods of volume calculation now approaches agreement to within approximately 20%. In detailed examination, no significant variation was observed with screen ruling, stylus angle or compression ratio. As an example, the data for screen ruling is shown below, (Graph 4.3)

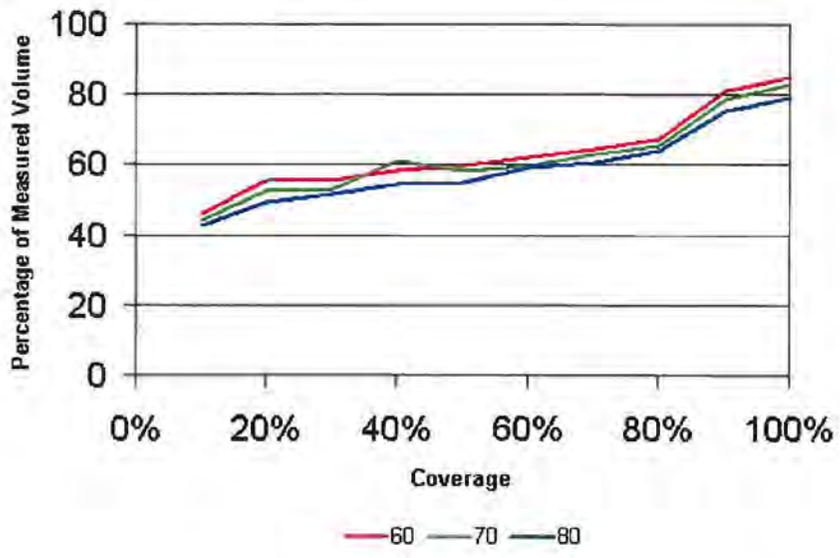

Graph 4.3 – Effects of screen ruling on ideal / measured volume deviation

As set out in 3.2.10, the cell volume may also be estimated by assessing a cone fit based on geometric parameters. The latter are derived from the image processing of the cylinder surface to measure the length and width of the cells. These are then averaged to give a calculated diameter for the cone, the volume of which is then calculated using the stylus angle, Equation 3.4. The application of this model is shown in Graph 4.3.

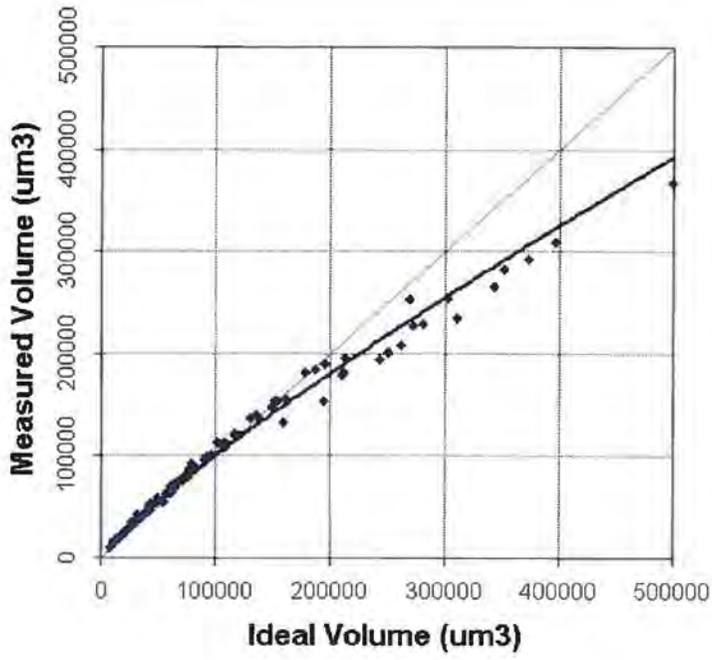

Graph 4.4 - Comparison of ideal volume and measured volume using conical calculation (Results for 60, 70, 80lpcm, 37, 45, 57° compression ratio, 120, 130, 140° stylus angle – all combinations)

Clearly this model produces results that are significantly closer to the measured data than those produced by the traditional pyramid model. It does however overestimate values above approximately 80% coverage. Overall it is significantly closer than the traditional pyramid model and this is confirmed in Graph 4.5.

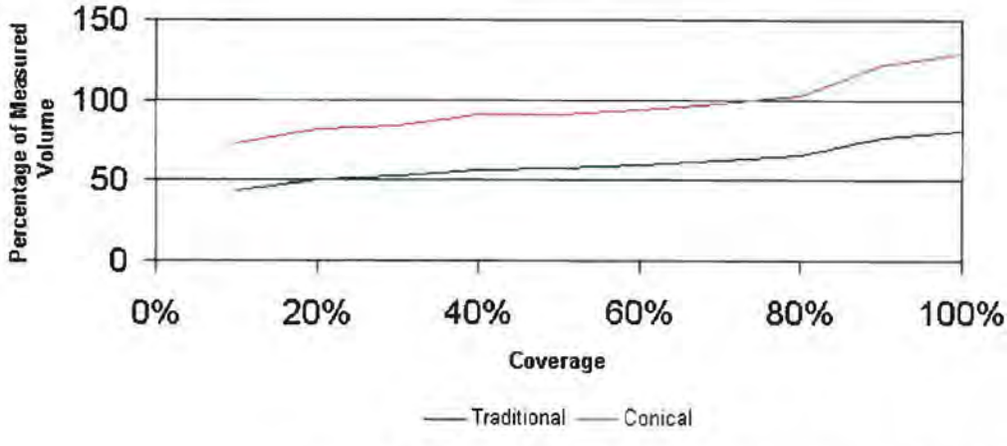

Graph 4.5 – Comparison of traditional and conical models

Although the shape is almost identical, the conical model is offset above the traditional data. Between 75-80% coverage the measurements and the conical model intersect. As an assurance check it may be possible to use this convergence to more accurately estimate cell volumes by measuring key parameters for 75% cells using image processing, and by applying the conical model. No variation was observed with screen ruling, stylus angle or compression ratio.

4.2.1 Summary

It has been shown that traditional methods of cell volume calculation are not accurate and underestimate. This is particularly the case at low coverages where errors of up to 60% of actual volume are observed, while errors of 30% are observed at higher coverages. A new model for volume estimation has been demonstrated, based on conical volume calculation, which is significantly more accurate than the traditional pyramid model when compared with the actual measured values.

All cell volume values used in the remainder of this thesis are measured values unless explicitly stated otherwise.

4.3 Cylinder Analysis

The cylinder was specified in terms of screen ruling, stylus angle and compression ratio. These quantities were measured and analysed to examine their effects on the print in terms of the colour and the ink released. As an example **Figure 4-1** illustrates the effects of changing screen ruling and compression ratio on the shape of the cells. As screen ruling is increased, the proportions of the cells remain constant, but the size and spacing between cells decreases. As compression ratio increases the cells move from being 'short and fat' to being 'long and thin'. The variation of compression ratio is used for the different colours in the four colour process, with cyan normally applied at a low compression ratio (37°±), yellow at 45°, and magenta at a higher compression ratio (57°±). Screen rulings are normally varied as well, with cyan and magenta often

having consistent screen rulings, yellow using a coarser screen (as yellow is less easy to see) and black using a finer screen (easy to see, and used for fine work, such as text). All examples shown represent cells at 30% tonal coverage. The bottom three diagrams show three different stylus angles at 70lpcm and 45°.

.

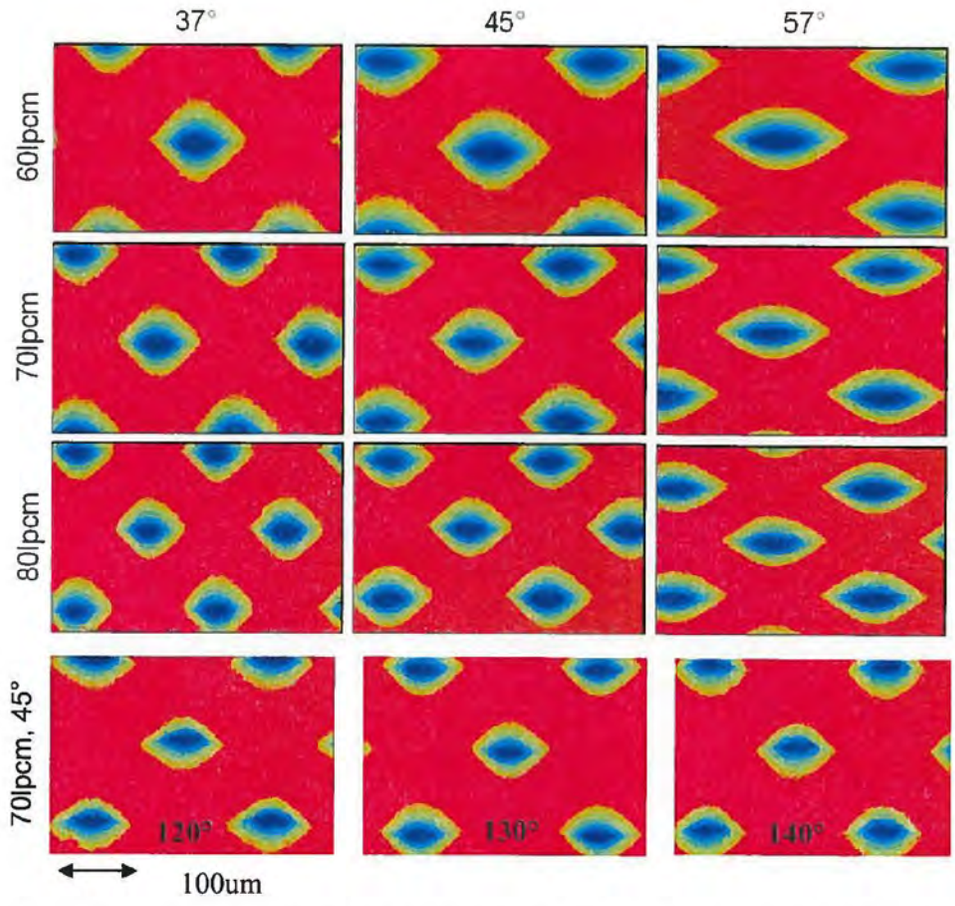

Figure 4-1 – Screen ruling / compression ratio comparisons (20x magnification)

The following sections, in order of presentation now focus on the effect of screen ruling, compression ratio and stylus angle.

4.3.1 Screen ruling

When changing the screen ruling of the engraving, the intention of the engraver is to produce geometrically similar cells, merely scaled up or down, depending on whether the engraver has decreased or increased the screen ruling. This section will investigate

the impact of screen ruling both in terms of the printed results, and in terms of cell engraved geometry.

The effects of screen ruling on the cell shape can be seen in Figure 4-1. It can be clearly seen that the shape of the cells does not change as the screen ruling is varied, although the size and spacing of the cells does. As previously stated, the engraver attempts to maintain the geometric shape of the cells when varying screen ruling, whilst varying the size and spacing of the cells. This has a significant impact on print density and example measurements derived from the orthogonal array matrix are shown in Graph 4.6.

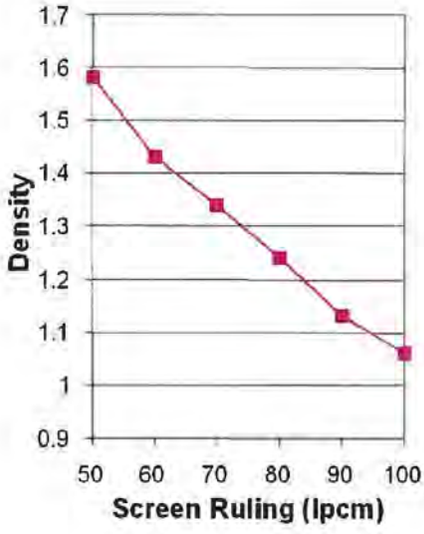

Graph 4.6 – Effects of screen ruling on solid density

Graph 4.6 shows that as the screen ruling of the engraving is increased, the solid printed density decreases. This trend is repeated irrespective of stylus angle, compression ratio or ink type. This decrease is approximately linear and is consistent over the range of screen rulings used by most gravure printers. This decrease in density may be explained by the reduction in specific volume observed when the screen ruling is increased - Figure 4-2.

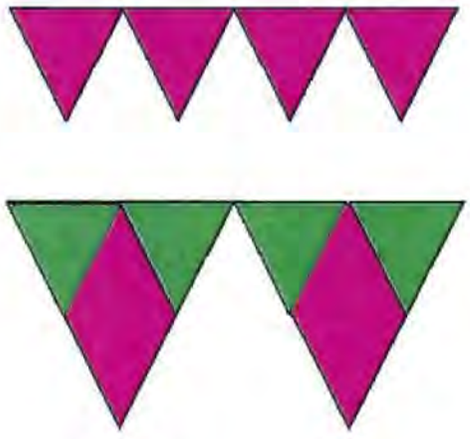

High Screen Ruling

Low screen ruling (magenta) with high screen ruling superimposed (green)

Figure 4-2 – Screen ruling comparison

Figure 4-2 shows two idealised screen rulings for 100% coverage. The top figure showing a screen ruling twice as high as the second screen ruling. In this case, each cell at the lower screen ruling is eight times larger than that of the higher screen ruling, and therefore the specific volume is doubled, thus accounting for the significantly higher solid densities measured at the lower screen rulings.

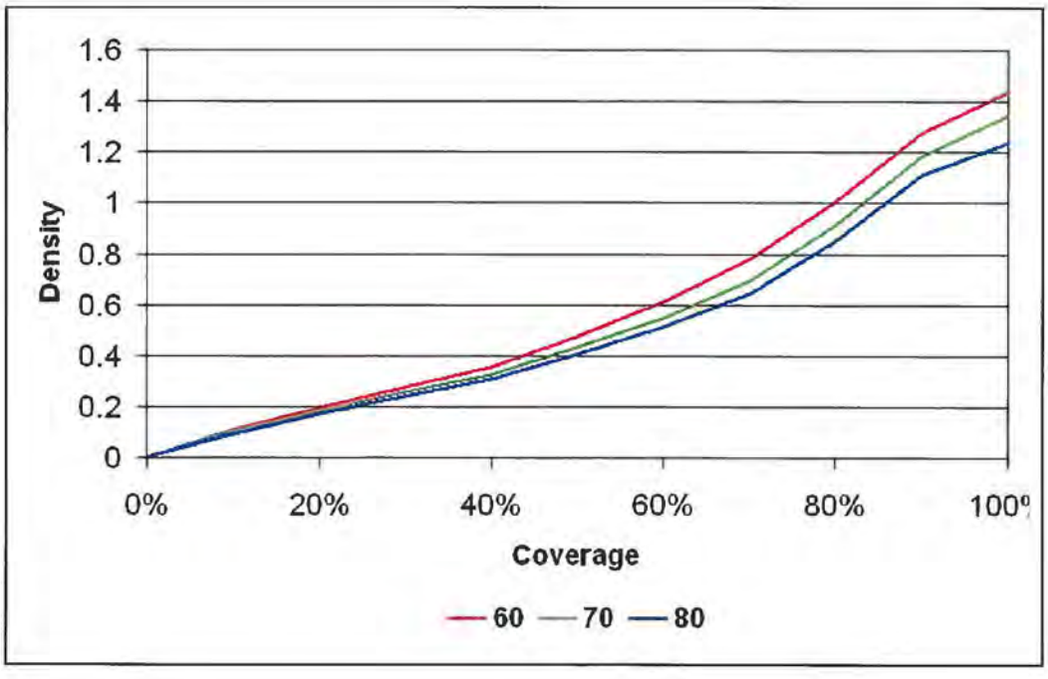

Graph 4.7 – Density and screen ruling with coverage. Results from orthogonal array matrices including averaged effects of compression ratio and stylus angle

Graph 4.7 shows the relationship between screen ruling, density and coverage. The elevated densities at lower screen rulings identified in Graph 4.6 can be clearly seen. The non linearity of the curve is due to the gamma curve that has been applied to the engraving in order to attempt to produce a visually linear print (once tone gain has been accounted for)[11].

Graph 4.8a shows the relationship between measured volume and screen ruling illustrating a characteristic that may be mapped using a power law. If the log of volume is plotted, it therefore follows that a straight line is produced. Density is also a logarithmic variable and Graph 4.8b shows density and log of volume plotted together as a function of screen ruling. The non-parallel nature of the two curves indicates the importance of something other than cell volume in determining the final printed density. This was attributed to the process of ink release and is the first evidence of the importance of this phenomenon.

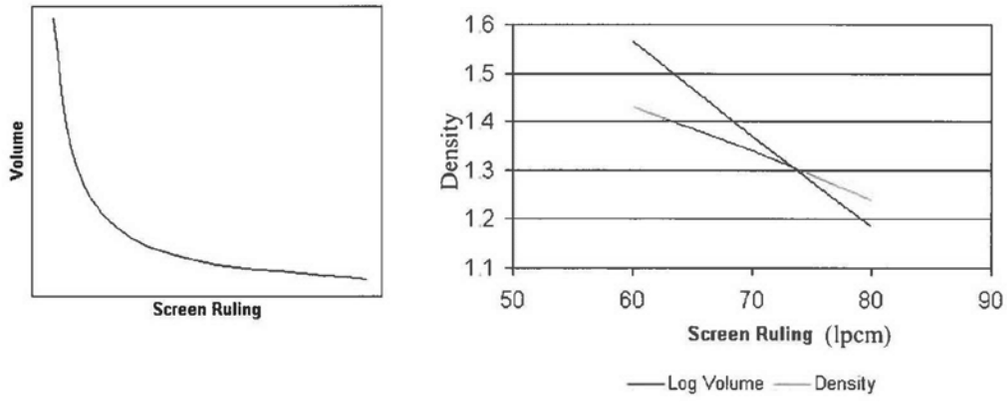

Graph 4.8 – Screen ruling – log volumes and densities[12]

[11] A direct linear increase in density leads to unacceptably large levels of tone gain in the mid ranges of coverage.

[12] The printed densities observed are generally lower than would be expected under production conditions, but in practice, the inks used would be modified according to the screen ruling used, in order to raise the maximum density of higher screen rulings to an acceptable level, by varying the pigment quantity in the ink.

To explore further the relationship between volume and density data was plotted for the three screen rulings. This however, gave a distinct curve for each screen ruling (Graph 4.9).

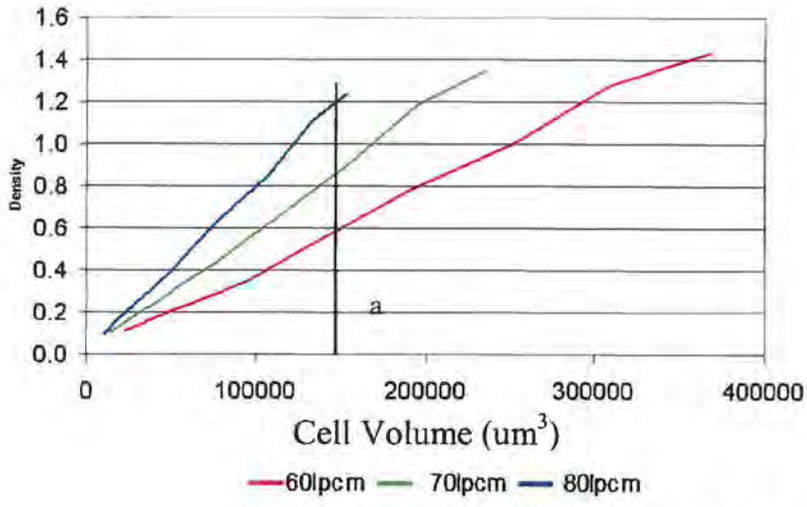

Graph 4.9 – Volume and Density

This graph demonstrates the clear correlation between cell volume and printed density, larger cells ultimately producing higher printed densities and three curves are observed. The line indicated 'a' in Graph 4.9 indicates a cell volume of approximately 150,000um^3. This equates to coverage of approximately 100% (80lpcm), 60% (70lpcm) or 40% (60lpcm). Unsurprisingly a 40%, 60lpcm patch will have a lower density than that of a 100%, 80lpcm patch. Although the cells are of similar sizes, significant space exists around the 40% cell. Following this result, density was replotted against specific volume ($\mu m^3/m^2$) - Graph 4.10, below.

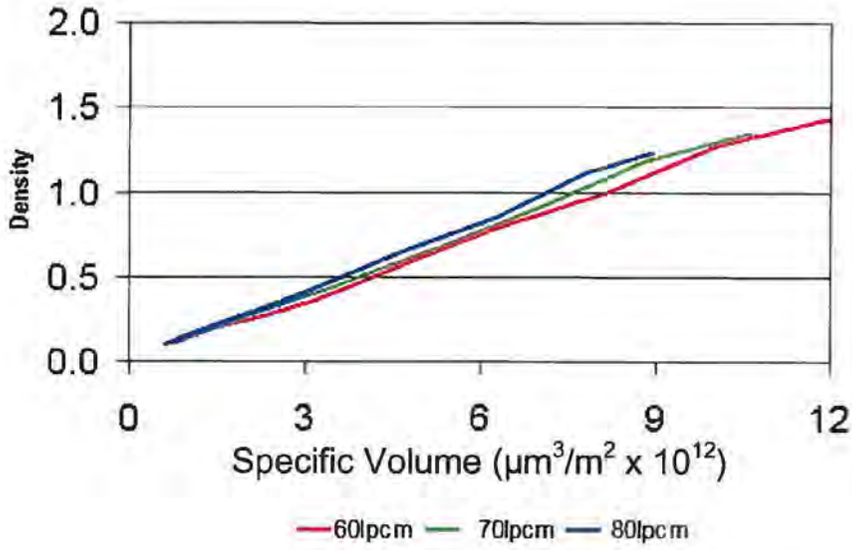

Graph 4.10 – Comparison of Specific volume and density

Comparing density with specific volume, it can be seen that the three curves plotted for the three screen rulings under consideration are grouped closely around a single line. Generally the trend between density and specific volume is a linear increase, with the curves extending further as the screen ruling decreases, due to the higher maximum specific volumes available to the lower screen rulings. In examining the details, it can also be seen that as screen ruling increases, there is a very small increase in the printed density for any given specific cell volume. This is attributed to the higher maximum densities available to the lower screen rulings. As a result of this, although the data is much closer, there are still differences in the specific volume / coverage relationship, and a 60lpcm screen ruling will still be delivering a lower coverage than an 80lpcm screen ruling for the same specific volume. This is, however, the same trend that is observed in terms of the ink release, where increasing the screen ruling increases the percentage of ink released from the cells, and as such the release is likely to be the primary factor causing this non-linearity in response between the screen rulings. This will be discussed further in Section 4.5.

Having explored printed image density, it is now appropriate to consider engraving issues and the impact of screen ruling more closely. When the cylinder was engraved, a Gamma curve was applied, and this was determined empirically by the engraver. This was used to ensure that printing will be achieved over the fullest range of

coverage. If no gamma curve is applied, it is likely that no ink will be printed below 20/25% ideal coverage and that '100%' actual coverage will be achieved above approximately 70% ideal coverage. Thus the effects of tone gain are compensated for, ideally leading to a gradation that is linear when measured optically. [13]

To explore the impact of the Gamma curve correction, measured cell volume is plotted against coverage for each screen ruling in Graph 4.11

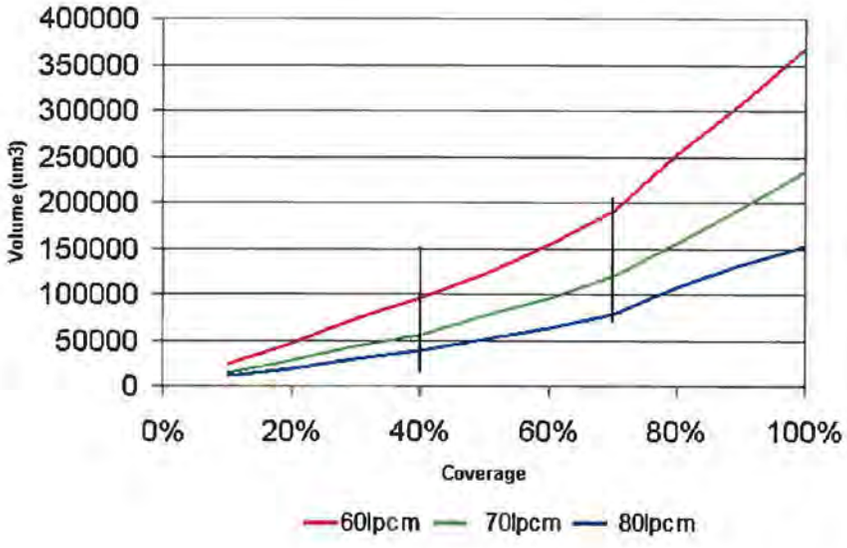

Graph 4.11 – Cell volume and coverage

This graph is divided into three segments in which it can be seen that volume increases, approximately linearly. Further examination was carried out, by plotting the actual percentage volume, compared with the 100% value. This can be seen in Graph 4.12 and the same trends are observed.

[13] Practically, different gamma curves are required for different substrates (ink transfer conditions), compression ratios, screen rulings, stylus angles, and as such, a standardised curve will never quite fit all conditions on the cylinder to achieve a fully optimised print.

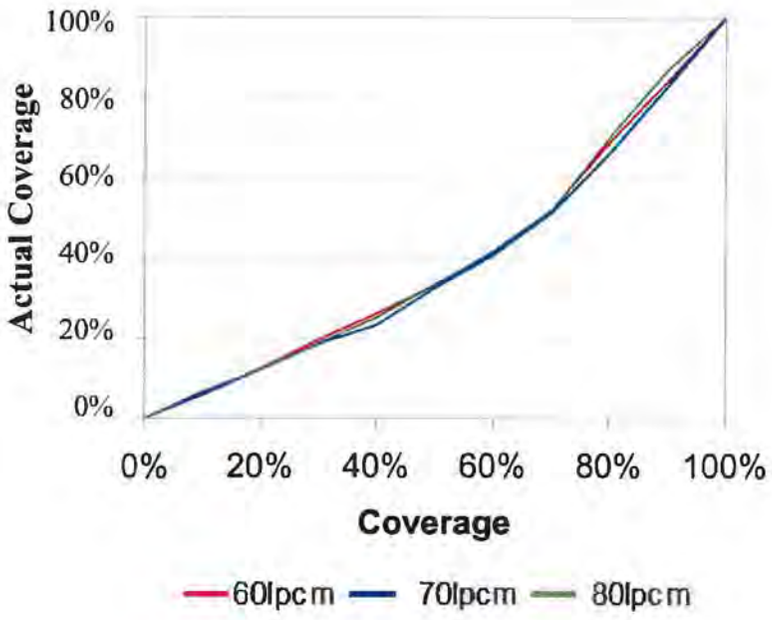

Graph 4.12 – Coverage against Percentage of max volume

The lower actual value compared with the ideal coverage reflects the ability to enable printing across the full tonal range. Maximum differences occur at approximately 60% ideal coverage, which shows a 20% deviation from the actual coverage.

Further analysis was undertaken to examine how the physical dimensions of the cells varied as screen ruling was altered. The graphs below illustrate this data in absolute terms across the coverage spectrum.

Graph 4.13 shows the effect of changing the screen ruling on the measured cell depth In the graph, 70lpcm is used as a reference, and the other screen rulings (60lpcm, 80lpcm) are shown as percentage difference.

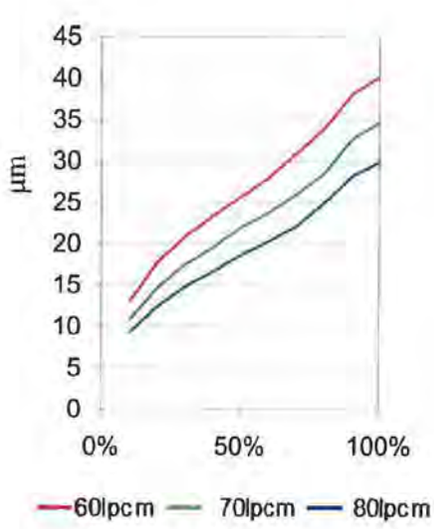

Absolute Values (A)

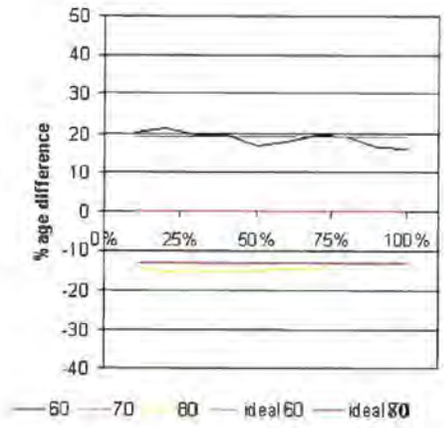

Percentage differences (B)

Graph 4.13 – Screen ruling – depth of cells

The graph of depth (Graph 4.13a) demonstrates that as screen ruling is increased, the depths of cells engraved decreases in an approximately linear fashion. The non-linearity in the curves with coverage is attributed to the Gamma curve applied to the engraving.

The effect of increasing the screen ruling from 70 to 80 lpcm is to decrease the depth of the cells, by approximately 14% from that observed in 70lpcm cells across the coverage, from 10% to 100%. Decreasing the screen ruling from 70 to 60 lpcm increases the depth of cells by approximately 20%. This also remains constant across the coverage from 10% to 100%. This trend is repeated for width and length. Open area shows the same trend, although with different values, with 60lpcm giving approximately 40% more open area than 70lpcm, and 80lpcm giving approximately 25% less (generally ±2%). The 'ideal 60' and 'ideal 80' show the depth of a cell if calculated from its width (in the traditional manner). It is clear that the measured depths are approximately equal to the ideal depths.

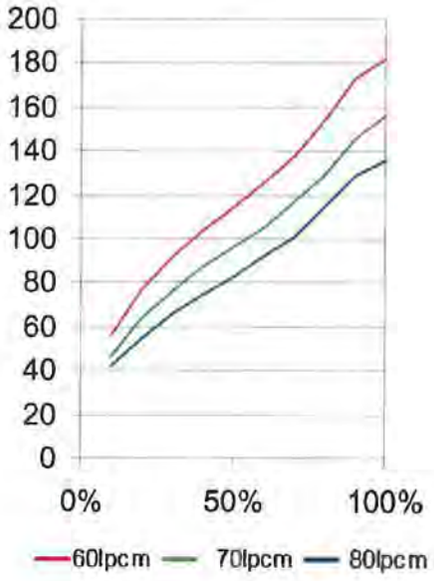

Graph 4.14 – Width measurement with screen ruling. Results from orthogonal array matrix and averaged for stylus angle and compression ratio

The width curves (Graph 4.14) are identical to the depth curves (Graph 4.13) and this is due to the hardness of the diamond. As the diamond does not deform as it cuts the cells, the depth and width of the cells are directly linked, both to each other, and to the stylus angle of the diamond. This relationship between the depth and width of the cells has led to the traditional method of depth inference from the stylus angle / width correlation. This assumes that there is no elastic recovery of the copper after engraving, that the stylus angle of the diamond is fixed at its defined angle, and that no wear has occurred. There is no simple method, however, to ascertain whether these assumptions are valid.[14] It should be noted that in these graphs of physical parameters , the plots have not been extended below 10% as below this point, the curves are

[14] A method was developed to analyse diamond stylus angles, and is detailed in the appendices. This confirms the variability that occurs between nominally identical diamonds, and that once a diamond has been used, the angle may vary by anything up to 10° from the specified value. Due to the nature of this work, the effects are not critical, as measurement of the cells themselves has been performed, however this will lead to significant variations between measured and calculated volumes, typified by the trends shown in Graph 4.1.

likely to be highly non-linear in order to allow the printing of a very-low coverage dot.

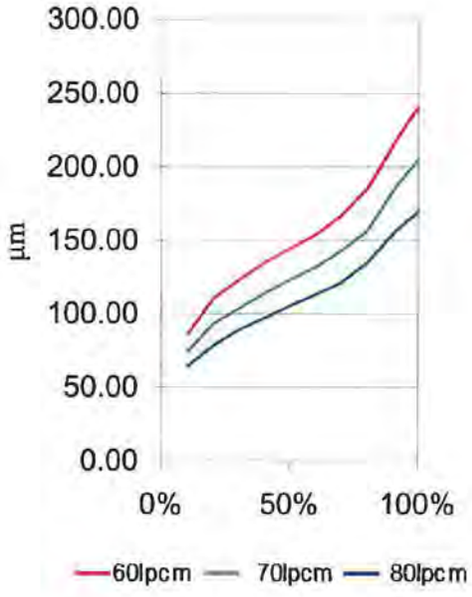

Graph 4.15a – Length

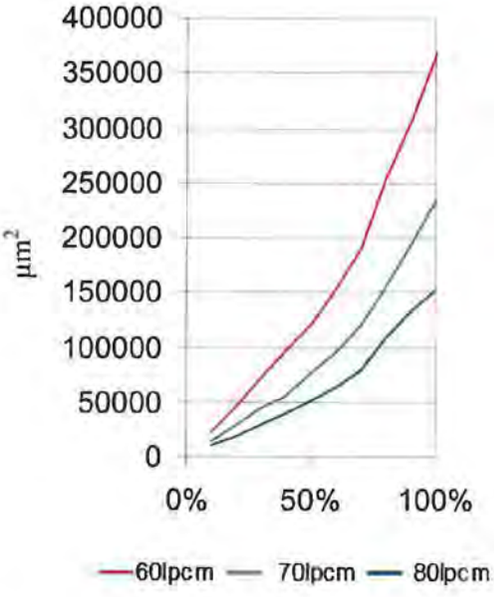

Graph 4.15b – Open area

Graph 4.15 – Effects of screen ruling

Graphs 4.14a and b detail the effects of screen ruling on the length and open area of the cells. As coverage increases and as screen ruling decreases, the length of the individual cells increases. This increase is approximately linear between the screen rulings, but is non-linear with respect to the coverage. Again, this is due to the Gamma curve being applied. Because the same curve was applied to all three screen rulings, the effects are the same at each coverage irrespective of screen ruling. However, it has introduced a non-linearity to the increase with coverage. As coverage increases, the open area increases, this being due to the increase in the size of the cells used for printing higher coverage areas. As screen ruling increases, the open area at each coverage decreases. This is due to the decrease in cell size as screen ruling increases – increasing screen ruling leads to improved resolution, smaller cells in general, and smaller open areas. This increase is non-linear both as the coverage increases, and between the screen rulings.

The upward trend in length, open area and volume above 80% coverage is caused by the purposeful introduction of channels joining the higher coverage cells together. These channels are included as it is believed that this improves ink release at higher levels of coverage. These channels are indicated in Figure 4-3.

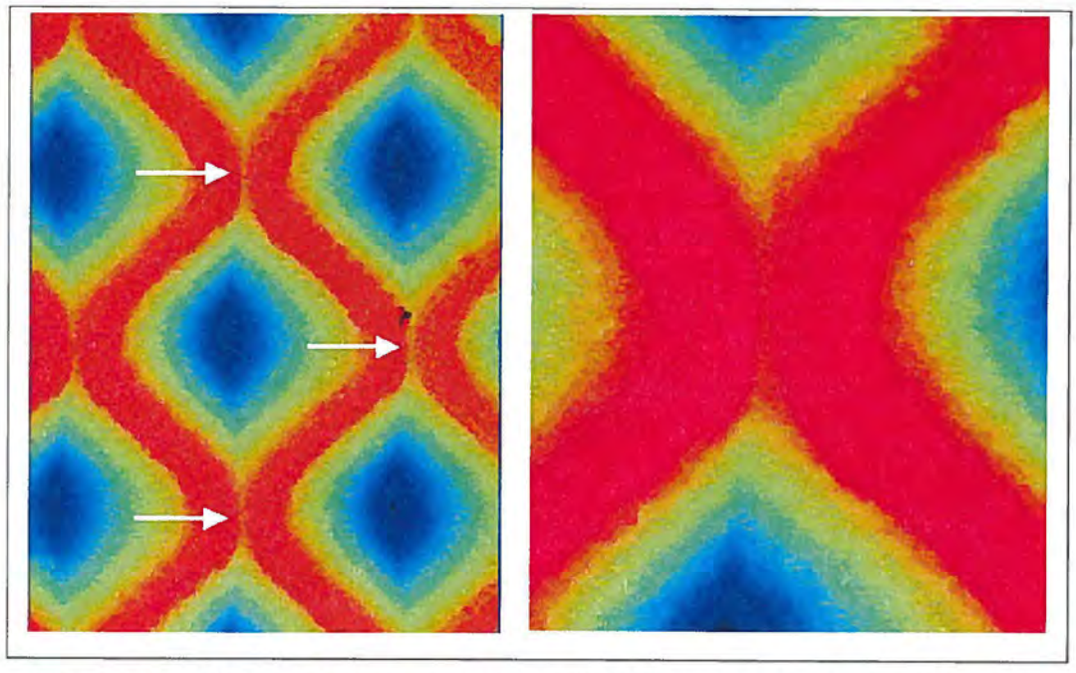

Figure 4-3 – Channels between gravure cells (45° compression ratio, 140° stylus, 80lpcm, 100% cells)

The effect of screen ruling on calculated tone gain was also examined, Graph 4.16, and the tone gain for all rulings is compared with 70lpcm.

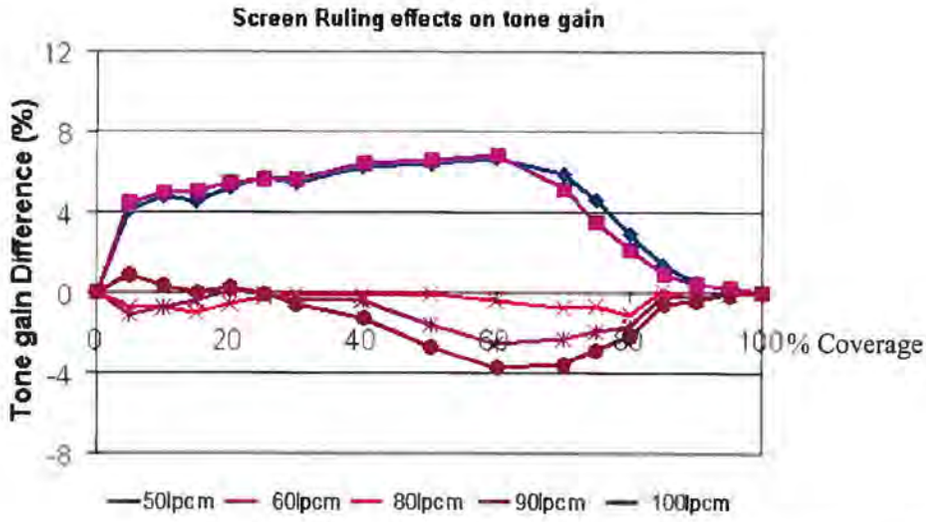

Graph 4.16 – Effects of screen ruling on tone gain

Rulings of 50lpcm and 60lpcm exhibit higher tone gain than 70lpcm, while 80lpcm, 90lpcm and 100lpcm exhibit decreased tone gain. The results for 50lpcm and 60lpcm are significantly higher than those at 70lpcm, whilst those at 80-100lpcm are much closer to the 70lpcm values. Although there is definitely a decrease in tone gain as screen ruling increases, the response is non-linear, irrespective of compression ratio, stylus angle and ink type. It is probable that this is due to the Gamma curve being optimised for the higher screen rulings, but there is no way to quantify this, and such optimisation remains an issue for further study to establish a clear understanding.

Physical tone gain of the sample was also considered over the tonal region being analysed, Graph 4.17. At 60lpcm, significantly higher physical dot gain is observed. This is likely to be due to the extremely low viscosity nature of the ink, where larger dots are more able to spread out. This is supported by the observations limiting the measurements of transferred volume. When lower viscosity inks are used, the dots join up much earlier (often at 60% coverage) thus making the analysis of individual dots impossible. At higher viscosities however, the dots remain individual to at least 60% and in certain cases as far as 80% coverage. Due to the necessary transparency of the ink (required for process colours to allow overprinting, and thus the creation of extra hues than those provided for by the individual inks) it is believed that this spreading has caused the optical density to be reduced due to the extremely thin ink layers observed.

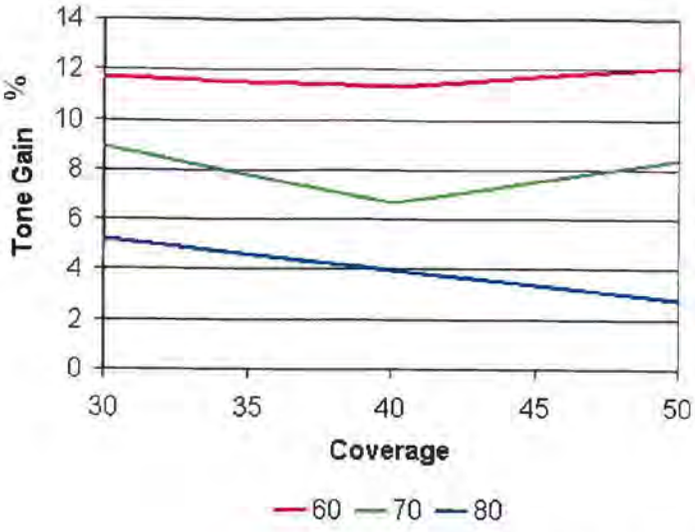

Graph 4.17 – Physical tone gain

This in turn leads to a lower tone gain, despite the significantly larger volumes of ink being transferred.

4.3.1.1 Screen ruling summary

As screen ruling increases, printed density decreases, both in terms of solids and of tonal reproduction. This is largely due to the reduced specific volume available at higher screen rulings. It was also observed that the increase in volume with coverage is non-linear, with two apparent regimes occurring. This was attributed to the failure of the applied Gamma curve to provide a linear increase. The depth, width, length and open area all decrease as screen ruling is increased. This decrease is consistent (proportionally) across the tonal range. Finally, as screen ruling increases, tone gain decreases. This has been attributed to the viscosity of the ink allowing larger dots to spread out further, which was borne out by analysis of the physical dot gain of the system.

The implications of this are that the shape of engraving, generally, fits the idealised calculations, in terms of the length, width etc. As such volume deviations are as a consequence of the cell shape, rather than its dimensions, and are caused by non-

straight sides and the internal shape of the cell itself. This confirms the need for the use of white-light interferometry as a technique for analysis of the cells.

4.3.2 Compression ratio

In the other major printing processes (lithography, flexography, screen printing) it is possible to simply vary the screen angle either digitally, or by rotating film screens to eliminate problems with Moiré. This is not possible with rotogravure printing, due to the engraving technique. In electromechanical engraving, a sinusoidal signal is applied to the diamond, forcing it into and pulling it out of the cells at approximately 4000Hz representing a cycle time of 250μs. The actual engagement time may be constant (if engraving 100% cells with channels) or as low as 20μs in areas of low coverage. Thus, by changing the signal applied to the engraving diamond, coupled with the rotation of the cylinder, it is possible to produce either short, fat cells (reduced compression ratio – lower screen angles) or long, thin cells (increased compression ratio – higher screen angles). To engrave shorter cells, the rotation of the cylinder is speeded up, and the amplitude of the engraving signal is increased. This produces shorter, deeper cells. To engrave longer cells, the cylinder rotation is slowed, and a lower amplitude signal is applied. This engraves longer cells (due to the increased contact time) but shallower cells (due to the decreased amplitude of the engraving stroke). These cells nestle closely, providing an alternative method of varying the screen angle, while maintaining the volume between different compression ratios. The effect of varying compression ratio on overall cell shape can be seen in Figure 4-1, where the effects of changing from a 37° compression ratio to a 45° compression ratio to a 57° compression ratio are shown. These are angles commonly used in the gravure industry.

An example of the effects of changing compression ratio on printed density as measured on the printed images, is shown in Graph 4.18.

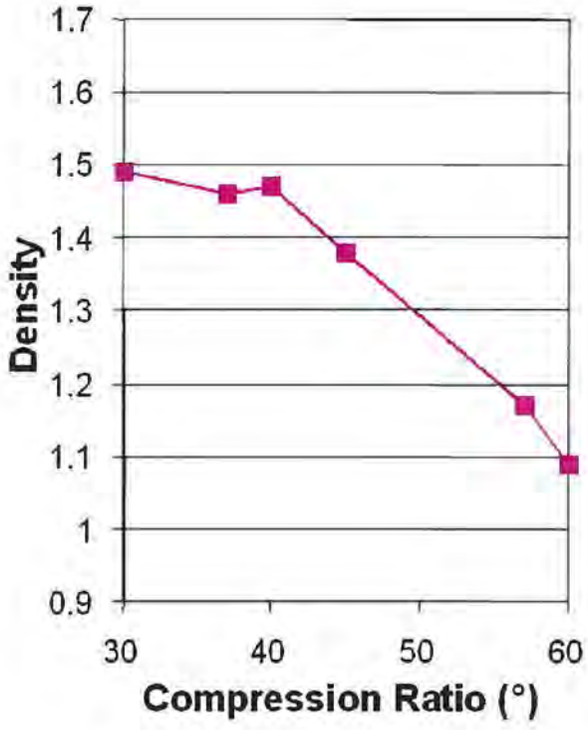

Graph 4.18 – Effects of compression ratio on solid density

As the compression ratio increases from 30° - 45° the solid density remains approximately constant, with only a slight decrease being observed (Graph 4.18). From 40° upwards however, an approximately linear decrease is observed. This trend was found to be present, irrespective of screen ruling and stylus angle. This is caused by changes in cell volume, and this will be discussed below.

The relationship between cell volume and printed density are shown in Graph 4.19. These results are from the orthogonal array matrix, and consist of averaged results from 60, 70 and 80lpcm screen rulings, and 120°, 130° and 140° stylus angles.

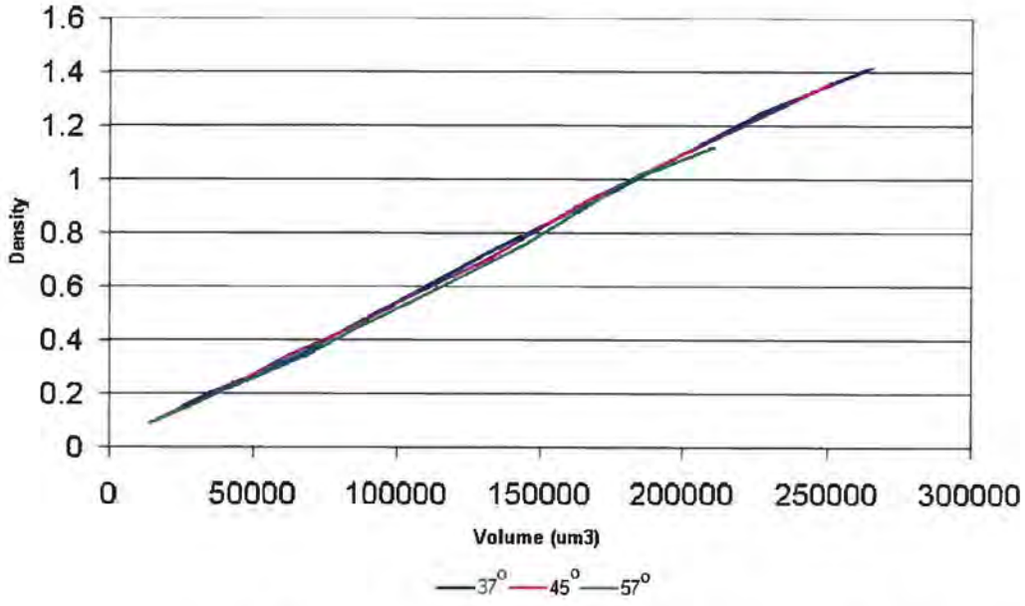

Graph 4.19 – Volume and Density. Results from orthogonal array matrix

It can be seen that as volume is increased, density increases linearly, and that no significant differences are observed at any point. This demonstrates that if all other variables are maintained constant (screen ruling, stylus angle etc), changing the compression ratio will not alter the printed density. However, as shown in Graph 4.18, altering the compression ratio has a non-linear impact on density and this implies that cell volume will be influenced by compression ratio, and this is shown in Graph 4.20.

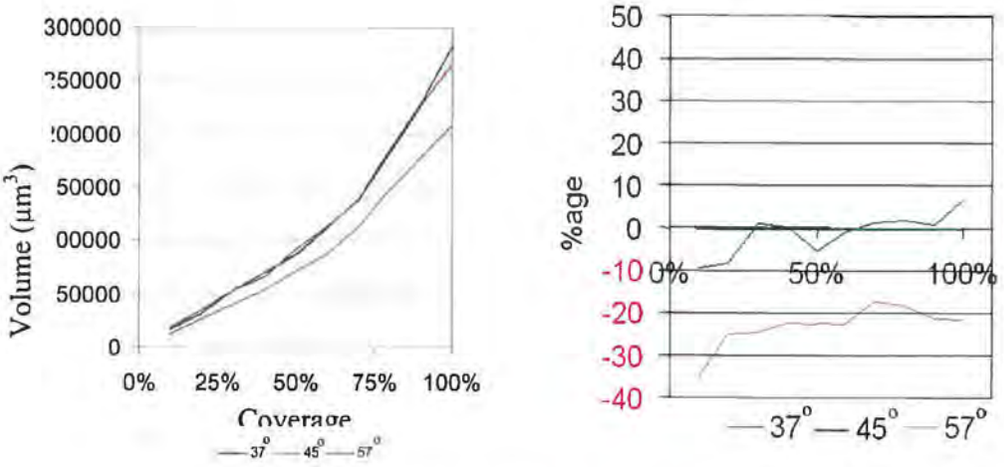

Graph 4.20 – Compression ratio effects on cell volume

The cell volume for 37° and 45° cells remains approximately constant, with differences up to 10% occurring. As compression ratio is increased further, the cell volume decreases significantly and proportionately with coverage. Also, no significant differences in trend are observed when recalculating in terms of specific volume. This is due to the number of cells per unit area remaining approximately constant as compression ratio is varied. This trend is repeated in the depth and width measurements, with only small changes being observed between 37° and 45°, but much larger changes being observed between 45° and 57°, as shown in Graph 4.21.

The effect of changing compression ratio is not consistent across the tonal range. In the highlight region (<20% coverage) both 37° and 57° engravings produce lower volume cells than 45° engravings (Graph 4.20). In the shadow regions, 37° engravings produce higher volume cells than 45° cells. A gradient appears to be present in both the 37° and 57° engraving curves. This can be attributed to the Gamma curve applied to the engraving, which was empirically derived for a 45° compression ratio.

Similar results were also observed, and have been discussed with respect to the solid printed density. Little change was observed between 37° and 45°, but a significant reduction in solid density was observed as the compression ratio was increased to 57°. This mirrors the trend for volume, and indicates the importance of cell volume as a dominant factor in printed density Graph 4.21.

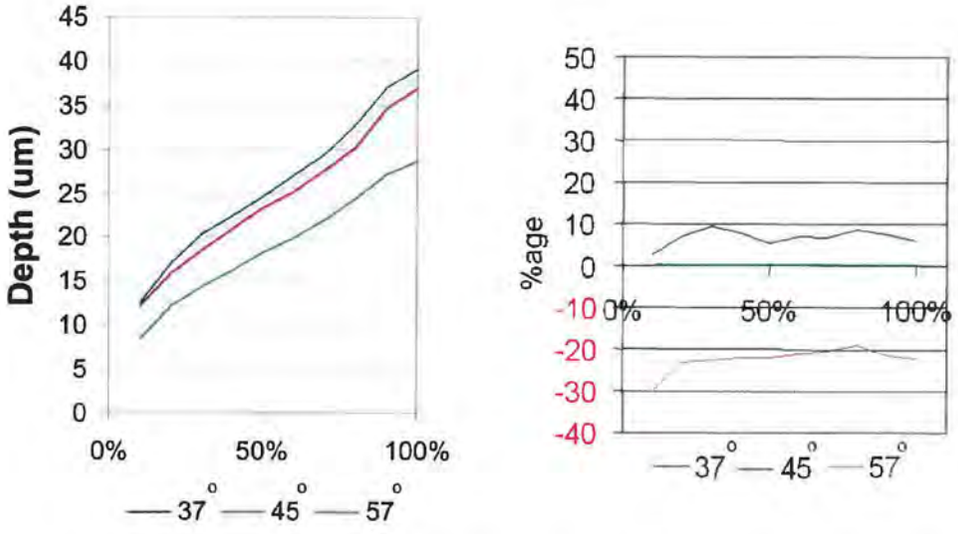

Graph 4.21 – Compression ratio effects on Depth. Results from orthogonal array matrices, averages for screen ruling and stylus angle. Magenta ink.

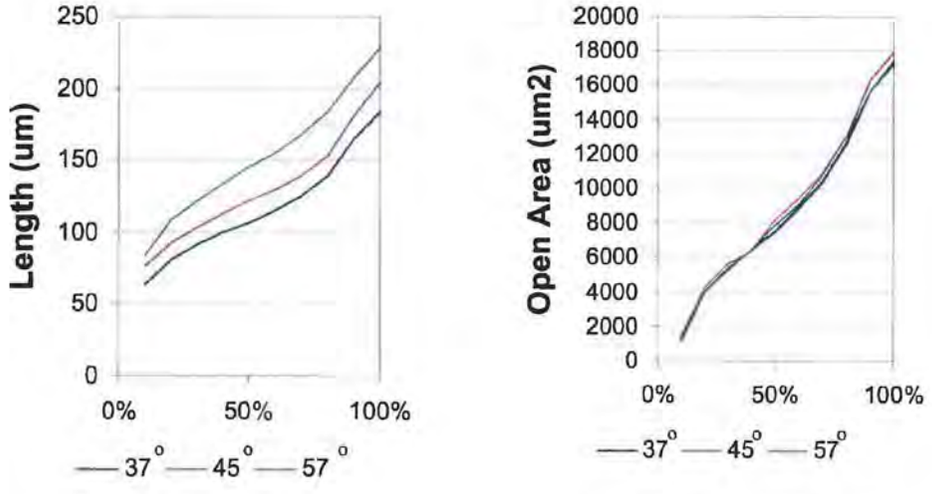

Graph 4.22a - Length

Graph 4.22b – Open area

Graph 4.22 – Compression ratio effects on cell length and open area

As compression ratio increases, the length of the cells increases (Graph 4.22a). This is for the same reason that the cell width decreases as compression ratio increases. To maintain a similar volume with a narrower cell, the length must be increased to compensate for this. A different trend is, however, observed in Graph 4.22b. As

compression ratio increases from 37° to 45° the cell open area increases slightly, while from 45° to 57° the cell open area decreases slightly. Thus an apparent optimum open area occurs at 45° compression ratio. Across much of the coverage range 37° and 57° engravings remain approximately consistent with an open area approximately 5% smaller than that observed with a 45° engraving. For a diamond shaped cell, the open area is;

$$\text{Area} = \frac{\text{Width} \times \text{Length}}{2}$$

Equation 4.1 – Area of a diamond

and this exhibits a maximum value when width and length are equal. However, this variation is very small.

Depth and width both demonstrate that 37° engravings produce deeper, wider cells across the entire coverage range than 45° engravings, which are in turn, deeper and wider than 57° cells. In each case, this increase / decrease remains approximately consistent across the coverage range. Depth and width are extremely closely linked because of the engraving mechanism (as discussed in 4.3.1), thus only depth results are shown, as the width shows an identical trend.

Open area shows similar trends to volume across the tonal range, in that both 37° and 57° engravings show significantly lower open areas than 45° engravings in the shadow regions, whilst all engraving angles have similar open areas in the shadow regions, albeit with 37° and 57° engravings demonstrating slightly lower open areas, Graph 4.22.

Length demonstrates the opposite trend. If the depth and width are decreased as compression ratio increases, then the length must therefore be increased to compensate for this.

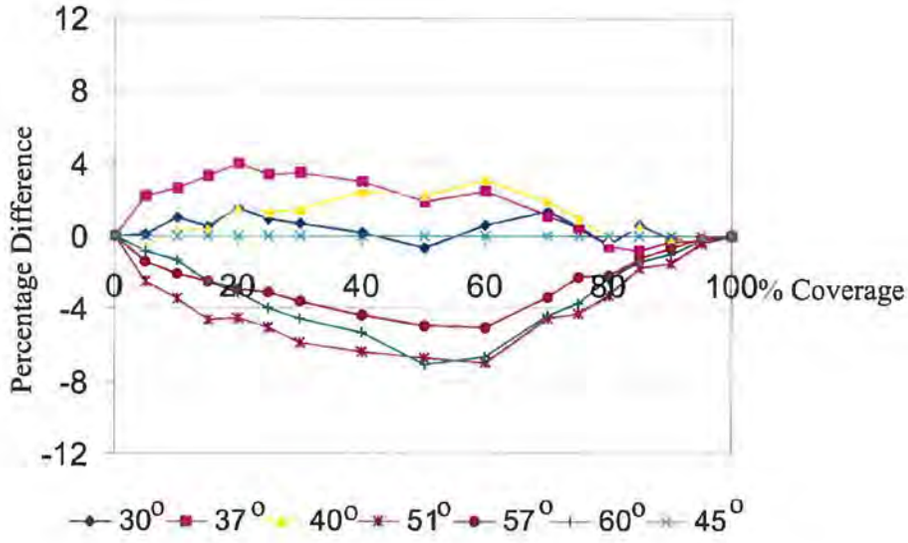

Graph 4.23 – Effects of compression ratio on tone gain

The effect of compression ratio on optical tone gain is shown in Graph 4.23. Generally there is a decrease as compression ratio is increased, which is shown further in Graph 4.24. It is also noted that from 30° to 45° smaller variations in tone gain are observed than above 45°. As with screen ruling, this can be attributed to the size of the printed dots, where the extremely low viscosity nature of the ink leads to the dots spreading out further, and thus increasing the optical dot gain further.

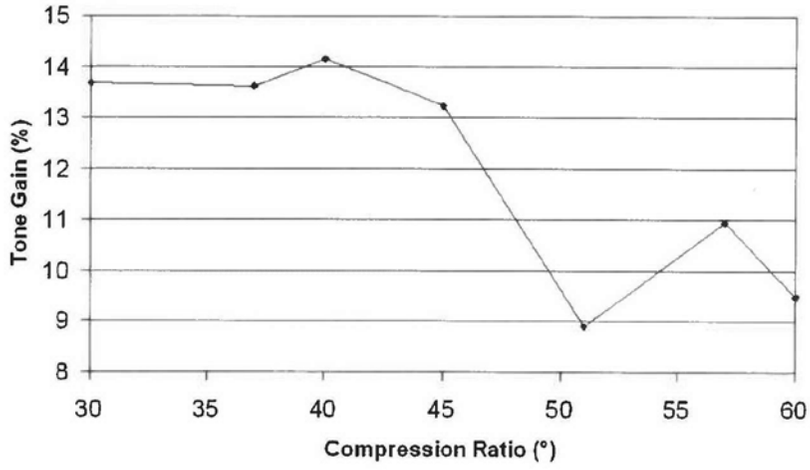

Graph 4.24 – Change in tone gain with compression ratio (70% coverage). Results from orthogonal array matrices – averaged screen ruling and stylus angle

Maximum deviations of the order of 8% are observed which is small but not insignificant. This again highlights the need for different gamma curves to be applied for different compression ratios.

4.3.2.1 Compression ratio summary

As compression ratio increases, the depth of the cells decreases along with the width, whilst the length of the cells increases, thus approximately maintaining volume, while allowing the external shape of the cells to be changed to approximate changing the screen angle, and thus allowing the prevention of Moiré. The open area of the cells reaches a maximum at 45° compression (where length and width are approximately equal). The printed density, both solid and in tonal regions decreases as compression ratio increases, although no significant difference is observed as the compression ratio is increased from 37° - 45°. This is because the volume remains approximately constant between 37° and 45° before decreasing as the compression ratio is increased beyond 45°.

Finally, if all other variables are maintained (including cell volume), then changing the compression ratio is not likely to affect the printed density.

4.3.3 Stylus angle

The stylus angle is the angle at the tip of the engraving diamond. Changing this angle will alter the internal dimensions of a cell, although the external dimensions must be maintained for the purposes of screening and Moiré elimination. The selection of a stylus angle will depend on many parameters. Small stylus angles produce larger cells (due to their more pointed nature), which will therefore transfer more ink, and are often used in the packaging industry, where the transfer of the maximum amount of ink possible is desirable (for the strongest, most vivid colours). The publication industry uses larger stylus angles. These styli last longer and produce smaller cells, minimising the amount of ink that is required to print the image.

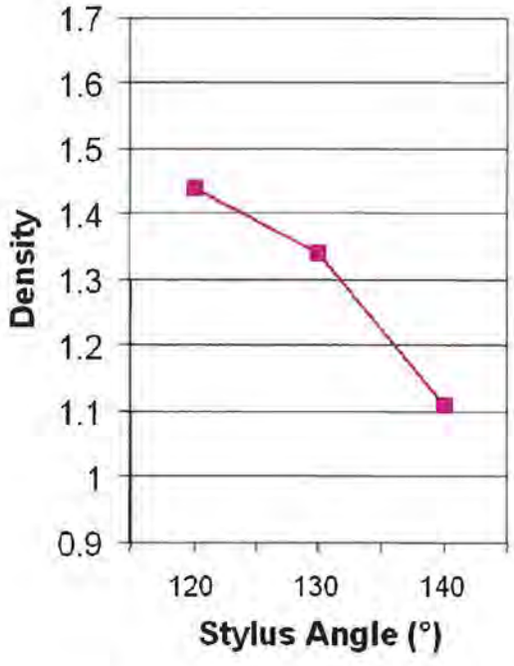

Graph 4.25 – Effects of stylus angle on solid density

Graph 4.25 shows that as stylus angle is increased, solid density decreases. This is largely due to the reduction in volume, which occurs as stylus angle increases.